Endogenous opioids gate the locus coeruleus pain generator

Makenzie R. Norris[1,2], Chao-Cheng Kuo[1], Jenny R. Kim[1], Samantha S. Dunn[1], Gustavo Borges[1], Loc V. Thang[1], Jordan G. McCall[1,2*]

[1]Department of Anesthesiology, Washington University in St. Louis, St. Louis, MO, USA; Department of Pharmaceutical and Administrative Sciences, St. Louis College of Pharmacy, St. Louis, MO, USA; Center for Clinical Pharmacology, St. Louis College of Pharmacy and Washington University School of Medicine, St. Louis, MO, USA; Washington University Pain Center, Washington University in St. Louis, St. Louis, MO, USA.

[2]Division of Biology and Biomedical Sciences, Washington University School of Medicine, St. Louis, MO, USA.

*To whom correspondence should be addressed:

J.G.M.: Address: 660 S. Euclid Ave, Box 8054, St. Louis, MO, USA, 63110. Phone: +1-314-446-8157. E-mail: jordangmccall@wustl.edu Website: www.mccall-lab.org.

Abstract

The locus coeruleus (LC) plays a paradoxical role in chronic pain. Although largely known as a potent source of endogenous analgesia, increasing evidence suggests injury can transform the LC into a chronic pain generator. We sought to clarify the role of this system in pain. Here, we show optogenetic inhibition of LC activity is acutely antinociceptive. Following long-term spared nerve injury, the same LC inhibition is analgesic – further supporting its pain generator function. To identify inhibitory substrates that may naturally serve this function, we turned to endogenous LC mu opioid receptors (LC-MOR). These receptors provide powerful LC inhibition and exogenous activation of LC-MOR is antinociceptive. We therefore hypothesized that endogenous LC-MOR-mediated inhibition is critical to how the LC modulates pain. Using cell type-selective conditional knockout and rescue of LC-MOR receptor signaling, we show these receptors bidirectionally regulate thermal and mechanical hyperalgesia – providing a functional gate on the LC pain generator.

Introduction

The role of the locus coeruleus-noradrenergic (LC-NE) system in chronic pain is both controversial and enigmatic. The LC-NE system is a powerful acute endogenous analgesia system(*1*), but evidence also suggests neuropathic injury converts this analgesia system into a system that sustains chronic pain, or in other words, a pain generator. Canonically, the LC modulates descending control of nociception via efferent projections to the dorsal horn of the spinal cord(*2*). Supporting this concept, spinal norepinephrine release from LC activation inhibits nociceptive inputs to the dorsal horn via activation of postsynaptic α2 adrenergic receptors(*3*). LC-mediated analgesia is further supported by studies showing that cell type- and projection-selective activation of these spinal projections is both antinociceptive and analgesic(*1*, *4*). Recent work, however, demonstrated that activation of LC projections to the deep spinal cord disrupted diffuse noxious inhibitory control of wide dynamic range neurons – a phenomenon thought to underly conditioned pain modulation(*5*, *6*). In this vein, work in human subjects has shown that LC activity is associated with the interaction between attention (increased visual sensory discrimination) and analgesia (diminished nociceptive percept)(*7*). The role of the LC in pain becomes further complicated when incorporating studies that disrupt its normal function. In

particular, lesioning the LC following neuropathic injury can reverse mechanical hypersensitivity(*8*, *9*) – suggesting some role in maintaining chronic neuropathic pain. While there is evidence that neuropathic injury induces neural plasticity and differential gene expression in LC neurons(*10*), it is not immediately clear how these plastic changes convert an analgesic system into a pain generator.

The apparently contradicting role of LC in pain may be due in part to the functional heterogeneity within the LC(*11*). Traditionally the LC has been thought of as a mostly homogenous brainstem structure due to its nearly ubiquitous expression of somatic norepinephrine, vast efferent system(*12*), and gap junction coupling between LC neurons(*13*). However, a growing body of evidence is rapidly redefining this important neuromodulatory system(*4*, *12*, *14–17*). For example, in rats with neuropathic injury, while chemogenetic activation of LC-NE neurons projecting to the spinal cord expectedly reversed allodynia, activation of LC-NE projections to the medial prefrontal cortex conversely increased spontaneous pain behaviors(*4*). Similarly, extensive work has shown that LC-mediated pain-induced negative affective and cognitive behaviors can be isolated from sensory modulation through distinct projections to the basolateral amygdala, anterior cingulate, hippocampus, dorsal reticular nucleus, and spinal cord(*18–21*). While most heterogeneity in the LC has been described in terms of efferent projections, emerging evidence also points to important afferent input to the LC in pain-related behaviors(*22–24*).

This afferent control of the LC is mediated through various cell-surface receptors. To that end, LC mu opioid receptors (LC-MOR) have also been implicated in changes to nociceptive processing. While it has long been postulated that LC-MOR dampen the stress response in these neurons(*25–30*), the endogenous MOR ligand met-enkephalin also induces antinociception when infused in the LC during the tail flick test(*31*). Likewise, LC infusion of the highly selective MOR agonist [D-Ala2, N-MePhe4, Gly-ol]-enkephalin (DAMGO) induces thermal antinociception. This DAMGO-mediated antinociception is reduced during persistent inflammatory pain, likely from the downregulation of LC-MOR protein expression(*32*). Neuropathic injury has also been shown to decrease expression of *oprm1* (the gene coding for MOR) in the rat LC(*33*). Together, these studies suggest LC-MOR may be a critical component to LC control of nociceptive processing. Here, we show that loss of LC inhibition from endogenous opioids may underly sustained pain in injured animals. We use inhibitory optogenetics to isolate the role of LC during acute nociception and nociception following chronic nerve injury. Furthermore, using a conditional knockout approach, we show that LC-MOR expression is required for normal nociception, and that restoring either LC-MOR signaling or receptor expression reverses the hypersensitivity that is caused by spared nerve injury in mice. Together, these data suggest that disruption of LC-MOR-mediated inhibitory tone in the LC converts this analgesic system into a pain generator.

Results

High tonic LC activity during hot plate test is not necessary for stress-induced antinociception

Noradrenergic neurons within the LC-NE system canonically exhibit three distinct activation profiles: low tonic, high tonic, and phasic activity. These firing profiles function differently in determining behavioral flexibility to various environmental challenges. Low tonic LC discharge (1-2 Hz) is thought to be consistent with an awake state(*34*, *35*), whereas phasic bursts(*17*, *36*) results from distinct sensory stimuli(*34*, *37*, *38*). Our previous work, and that by others, has shown that high tonic LC activity (3-8 Hz) drives anxiety-like behavior in mice and rats(*14*, *21*, *39–42*). However, other studies have demonstrated that this same high tonic activation of LC neurons can be either antinociceptive or pronociceptive, depending on dorsal-ventral localization or efferent projection target(*1*, *4*). These observations led us to hypothesize that stress-induced high tonic LC-NE may lead to stress-induced antinociception. Indeed, we find that the same 30-minute

restraint stress that induces anxiety-like behavior(*39*) is also strongly antinociceptive in a hot plate test in mice (**Supplementary Fig. 1A&B**). To determine whether stress-induced high tonic LC activity was responsible for this stress-induced antinociception during noxious stimulation, we sought to use an inhibitory optogenetic approach in mice that was previously used to successfully silence rat LC neurons(*43*). To do so, we selectively expressed a soma-targeted anion-conducting channelrhodopsin (stGtACR2) in the LC of mice heterozygously expressing Cre recombinase in place of dopamine beta hydroxylase (*Dbh*^{Cre}::LC-stGtACR2). We first validated this approach with *ex vivo* electrophysiological recordings of locus coeruleus neurons (**Fig. 1A**). Here we show 470 nm activation of stGtACR2 efficiently suppresses spontaneous LC action potentials for up to 35 seconds, substantially longer than the 30-second cutoff we use to prevent tissue damage on the hot plate (**Fig. 1B&C; Supplementary Fig. 2A&B**). This photoinhibition was particularly efficient, with as little as 2 mW light providing complete inhibition of spontaneous LC firing (**Fig. 1D**). Furthermore, we show that this stGtACR2-mediated inhibition is sufficient to silence activity evoked from large current injections (**Fig. 1E&F**). These recordings suggest stGtACR2 can maintain complete silencing against substantial excitatory input, likely larger than physiological input to the LC *in vivo* during nociception(*44*). As might be expected from prior studies with stGtACR2(*43*, *45*–*47*), whole-cell and cell-attached recordings of stGtACR2 expressing locus coeruleus neurons show rebound firing immediately after blue light cessation (**Supplementary Fig. 2C&D**). This rebound activity, however, is unlikely to affect our behavioral tests, as behavior is recorded and tested exclusively during LC inhibition. To ensure a smooth transition from the restraint stress to hot plate testing, we outfitted mice with a head-fixation bracket around bilateral fiber optic implants above the LC (**Supplementary Fig. 3A**) and restrained animals by both head and body restraint–this approach yields similar antinociception to restraint with a conical tube alone (**Supplementary Fig. 3B**). With all this information in hand, we next created a new cohort of *Dbh*^{Cre}::LC-stGtACR2 and *Dbh*^{Cre}::LC-mCherry mice with the combined head-fixation bracket and bilateral fiber optic implants above the LC to test whether LC inhibition during the hot plate test could suppress stress-induced antinociception (**Fig. 1G**). Here, LC inhibition had no effect on either *Dbh*^{Cre}::LC-stGtACR2 or *Dbh*^{Cre}::LC-mCherry stress groups (**Fig. 1H**), suggesting that high tonic LC activity is not necessary for the stress-induced antinociception during noxious sensation. Instead, much to our surprise, LC inhibition in *Dbh*^{Cre}::LC-stGtACR2 no stress controls was significantly antinociceptive compared to *Dbh*^{Cre}::LC-mCherry no stress controls (**Fig. 1H**). These findings suggest that, perhaps more so than in stress states, basal LC activity is critical to normal nociception in naïve animals. We next sought to determine the extent of this contribution across multiple sensory modalities.

Intact locus coeruleus activity contributes to baseline hind paw sensory thresholds

While prior studies have shown that high tonic LC activation can be either antinociceptive or pronociceptive(*1*, *4*), these studies did not address the extent to which spontaneous LC activity may contribute to baseline nociceptive thresholds. To determine whether ongoing LC activity is required for baseline nociceptive thresholds in mice, we once again expressed Cre-dependent stGtACR2 or mCherry and implanted fiber optics bilaterally above the locus coeruleus of *Dbh*^{Cre} mice (*Dbh*^{Cre}::LC-stGtACR2 or *Dbh*^{Cre}::LC-mCherry) (**Fig. 2A**). To determine whether LC activity is required for normal hind paw sensory processing, we inhibited LC neurons during von Frey and Hargreaves tests. LC inhibition increased the force necessary to elicit a paw withdrawal in *Dbh*^{Cre}::LC-stGtACR2 compared to *Dbh*^{Cre}::LC-mCherry, suggesting LC activity is necessary to establish normal evoked mechanical thresholds (**Fig. 2B**). Similarly, when we repeated this approach using the Hargreaves test, LC inhibition also significantly increased thermal withdrawal thresholds **(Fig. 2C**). In these evoked tests, one possible alternative explanation is that LC inhibition produces sedation(*35*). However, mice were fully active in the hot plate test, and LC inhibition did not reduce locomotion in a real-time place preference test (**Supplementary Fig. 4**)

– in each case showing no signs of sedation. Taken together, these results indicate that spontaneous LC activity helps establish sensory thresholds across both thermal and mechanical domains.

Locus coeruleus inhibition is analgesic in a time-dependent manner

While LC inhibition increases thermal and mechanical thresholds in naïve mice, it is not immediately clear that this same inhibition would provide analgesia in a chronic pain state. To test this hypothesis, we next sought to determine whether the antinociceptive effect of LC inhibition was maintained following neuropathic injury. To do so, we used the spared nerve injury (SNI) model on these same mice, ligating the tibial and peroneal nerve to cause robust and prolonged mechanical hypersensitivity(*48*–*57*)(**Fig. 2D**). As expected, one week after SNI, both groups of animals were significantly hypersensitive on the injured limb (**Fig. 2E**). At this one-week timepoint, however, LC inhibition was no longer antinociceptive in the injured limb. Remarkably, this bilateral LC inhibition led to modest, but significant, hypersensitivity in the non-injured limb (**Fig. 2E**)**.** In contrast, four weeks after injury, LC inhibition-induced antinociception was significantly restored in the injured limb of *Dbh*^{Cre}::LC-stGtACR2 mice, and the contralateral hypersensitivity in the non-injured limb was no longer present (**Fig. 2F**). This reversal of mechanical hypersensitivity appears to be directly related to noxious sensation, as LC inhibition does not induce a place preference using real-time place testing, providing no evidence of reward from ongoing pain relief (**Supplementary Fig. 4**). These findings further highlight the complexity of LC-mediated analgesia, with both duration and site of injury showing evidence of adaptation over time. Importantly, the analgesic effect of LC inhibition four weeks after SNI is consistent with prior lesion studies that led to the pain generator hypothesis(*8*, *9*, *58*).

LC-MOR expression is critical for LC-mediated baseline nociceptive behaviors

Following the observation that exogenous LC inhibition alters nociception in mice, we sought to determine what endogenous inhibitory mechanisms might do the same. MOR are a clear candidate for such a purpose as they are inhibitory G-protein coupled receptors that are heavily expressed in LC neurons and provide potent inhibition when activated(**Fig. 3A**)(*25*, *59*–*63*). LC-MOR agonism is antinociceptive, and prior studies have suggested that inflammatory and neuropathic injuries decrease LC-MOR protein and *oprm1* gene expression in the LC(*32*, *33*, *64*). To determine whether LC-MOR are required for LC-mediated nociceptive control, we generated a noradrenergic neuron-selective conditional knockout mouse through multiple generations of breeding between *Dbh*$^{Cre+/-}$ mice and mice with *loxP* sites on either side of exons 2-3 of the *oprm1* gene (*Oprm1*$^{fl/fl}$)(**Fig. 3B**)(*65*). After reaching *Oprm1*$^{fl/fl}$ homozygosity, *Oprm1*$^{fl/fl}$x*Dbh*$^{Cre+/-}$ LC neurons lose DAMGO-mediated inhibition (**Fig. 3C&D**), consistent with functional disruption of MOR in these cells. Importantly, this LC-MOR deletion does not lead to compensatory changes in spontaneous firing, rheobase, excitability, or input resistance in these cells (**Fig. 3E-H**). We next sought to determine whether *Oprm1*$^{fl/fl}$x*Dbh*$^{Cre+/-}$ mice have normally preserved nociceptive behavioral outputs. To do so, we performed von Frey and Hargreaves' testing to determine mechanical and thermal withdrawal thresholds, respectively, in these mice compared to Cre negative controls (*Oprm1*$^{fl/fl}$x*Dbh*$^{Cre-/-}$). We found *Oprm1*$^{fl/fl}$x*Dbh*$^{Cre+/-}$ mice have significantly decreased mechanical and thermal thresholds, suggesting that noradrenergic MOR expression is required for LC-mediated nociceptive thresholds (**Fig. 3I&J**). This finding is particularly notable given that global MOR deletion (*oprm1*$^{-/-}$ mice) decreases thermal nociception and prevents the antinociceptive effects of morphine(*66*, *67*) (**Supplementary Fig. 5A-C**). This difference aligns with the idea that MOR expression outside of noradrenergic cells is critical for typical MOR-mediated analgesia(*68*–*77*). Despite not detecting any compensatory changes in LC electrophysiological properties (**Fig. 3E-H**), Oprm1$^{fl/fl}$x*Dbh*$^{Cre+/-}$ have LC-MOR deleted throughout

development and it is possible that *oprm1* expression is perturbed in other *Dbh*+ cells. To control for these possibilities, we also bilaterally delivered AAV5-hSyn-eGFP-Cre anatomically to the LC of *oprm1*$^{fl/fl}$ mice (**Supplementary Fig. 6A**). This approach allows for conditional deletion of MOR expression in the LC during adulthood closer to the time of behavioral testing while also maintaining intact MOR expression during development and elsewhere in the body. This viral *oprm1*$^{fl/fl}$::LC conditional knockout had similar decreased baseline mechanical withdrawal thresholds to the *Oprm1*$^{fl/fl}$x*Dbh*$^{Cre+/-}$ mice (**Supplementary Fig. 6B**). Altogether, deletion of LC-MOR appears to cause a pronociceptive phenotype compared to mice with intact *oprm1* expression, suggesting LC-MOR contributes to LC control of nociception.

Restoration of MOR signaling in the LC reverses Oprm1$^{fl/fl}$xDbh^{Cre+} *pronociceptive phenotype*

Mice lacking MOR in the LC respond to lower levels of mechanical force and react more rapidly after the application of a noxious heat stimulus. To determine whether LC-MOR signaling itself is responsible for this pronociceptive phenotype, we used the light-sensitive chimeric opto-MOR receptor we previously helped develop(*78*). Opto-MOR allows for cell type- and intracellular signaling cascade-selective rescue of the G-coupled inhibitory signaling associated with MOR activation. Furthermore, due to its extracellular component unable to bind endogenous MOR ligands, it also leverages temporal control of signaling activation via photostimulation. To test whether this restoration of signaling would restore normal nociception, we used AAV5-Ef1α-DIO-OMOR-EYFP to selectively express opto-MOR in the LC of *Oprm1*$^{fl/fl}$x*Dbh*$^{Cre+/-}$ mice (**Fig. 4A&B**). We then bilaterally implanted fiber optics above the LC. Due to the extreme photosensitivity of the chimeric receptor, opaque black caps were used to prevent ambient light from entering the fiber optic ferrules between experiments. We had two different control groups for this experiment. For the first group, we expressed AAV5-Ef1α-DIO-OMOR-EYFP into the LC of Oprm1fl/flxDbhCre-/- mice, as these mice were unable to express the chimeric receptor due to the absence of the Cre recombinase. This group was needed to control for off-target effects of illumination in mice with normal nociception. The second control group expressed AAV5-Ef1α-DIO-EYFP in the LC of Oprm1fl/flxDbhCre+/- mice, as these MOR conditional knockouts maintain the pronociceptive phenotype while also experiencing viral delivery into LC. Opto-MOR activation in the LC of *Oprm1*$^{fl/fl}$x*Dbh*$^{Cre+/-}$ mice increased thermal paw withdrawal latencies in a light-dependent manner with no effect in either control group (**Fig. 4D**). Likewise, opto-MOR LC activation in the same *Oprm1*$^{fl/fl}$x*Dbh*$^{Cre+/-}$ mice also increased mechanical thresholds in the von Frey test (**Fig. 4E**). These findings suggest restoration of LC-MOR signaling alone is sufficient to reverse the pronociceptive phenotype in *Oprm1*$^{fl/fl}$x*Dbh*$^{Cre+/-}$ mice. Similar to when we inhibit LC activity in Dbh$^{Cre+/-}$ mice, we see no change in locomotion or real-time place preference from opto-MOR activation in *Oprm1*$^{fl/fl}$x*Dbh*$^{Cre+/-}$ mice (**Supplementary Fig. 7**). These data indicate that LC-MOR signaling directly alters thermal and mechanical thresholds.

Intra-LC MOR rescue in Oprm1$^{fl/fl}$x*Dbh*$^{Cre+/-}$ *mice reverses chronic neuropathic injury-induced hypersensitivity*

After discovering that LC-mediated baseline sensation is modulated by LC-MOR signaling, we next sought to determine whether full receptor rescue could reverse SNI-induced hypersensitivity. Although the *Oprm1*$^{fl/fl}$x*Dbh*$^{Cre+/-}$ mice lack LC-MOR, no modifications were explicitly made to endogenous opioid ligands. If these neuropeptides are still intact, then rescue of LC-MOR expression should mitigate SNI-induced hypersensitivity. This idea aligns with the previously observed decrease in LC *oprm1* expression after injury, altered opioid-induced activity, and decrease in LC-MOR protein after inflammatory pain(*32*, *33*, *64*). To test this hypothesis, we first bilaterally expressed the human OPRM1 gene in the LC of in *Oprm1*$^{fl/fl}$x*Dbh*$^{Cre+/-}$ mice (**Fig. 5A&B**) and demonstrated that this approach rescues DAMGO-induced LC inhibition in cell-attached

recordings (**Fig. 5C-E**). Notably, this inhibition through rescued hMOR expression falls into the physiological range provided by endogenous LC-MOR in the naïve LC (**Fig. 2C&D**), minimizing concern for under- or over-expression in subsequent behavioral experiments. To determine whether endogenous opioid ligands could then restore LC-MOR signaling, we next created a new cohort of *Oprm1*$^{fl/fl}$x*Dbh*$^{Cre+/-}$ mice and performed SNI or Sham surgeries on to induce long-term thermal and mechanical hypersensitivity (**Fig. 5F**). Eight weeks after SNI, *Oprm1*$^{fl/fl}$x*Dbh*$^{Cre+/-}$::SNI mice were mechanically and thermally hypersensitive compared to *Oprm1*$^{fl/fl}$x*Dbh*$^{Cre+/-}$::Sham controls (**Fig. 5G&H**). We then bilaterally expressed OPRM1(*79*) in the LC of both Sham and SNI *Oprm1*$^{fl/fl}$x*Dbh*$^{Cre+/-}$ mice and waited four weeks for expression of the rescued receptor. Remarkably, we found that hMOR expression in *Oprm1*$^{fl/fl}$x*Dbh*$^{Cre+/-}$::SNI mice completely reversed SNI-induced thermal and mechanical hypersensitivity with no clear effect on *Oprm1*$^{fl/fl}$x*Dbh*$^{Cre+/-}$::Sham controls (**Fig. 5G&H**). These data indicate that rescuing LC-MOR is sufficient for endogenous opioid ligands in the LC to blunt ongoing pain from nerve injury. Altogether, our results suggest LC-MOR-mediated inhibition is critical for evoked sensory responses and, without this LC-MOR-mediated inhibition, the LC generates pronociceptive behavior that can sustain chronic pain.

Discussion

The locus coeruleus noradrenergic system is well known as a key region in pain neural circuitry(*1*–*5*, *7*–*10*, *18*, *20*, *80*–*84*). Several studies have noted that the LC leverages its breadth of efferent circuitry to command robust control over nociceptive processing(*1*, *4*–*6*, *18*, *20*, *21*, *85*). Despite elegant previous work, the precise role the LC plays in pain control remains elusive, with clear evidence for both analgesia and generation of chronic pain(*1*, *4*, *5*, *8*, *9*, *86*). Several studies show the LC mediates acute antinociceptive effects when tonic activity is high(*1*, *4*, *20*, *85*). Here we demonstrate that spontaneous LC activity makes important contributions to the evoked responses from mechanical and noxious thermal stimuli. We first identified this phenomenon while testing the role of LC activity in stress-induced antinociception on the hot plate test (**Fig. 1H**). While this experiment found that LC inhibition during the hot plate test did not alter stress-induced antinociception, further work is necessary to identify whether LC activity during the stressor itself plays a role in restraint stress-induced antinociception. Additionally, we have shown that silencing of LC spontaneous activity under chronic neuropathic pain conditions reveals a time-dependent analgesic effect (**Fig. 2E&F**). While this observation aligns with other studies in rats where LC firing in response to noxious stimuli potentiated under neuropathic pain conditions after four weeks of injury, but not earlier(*87*), it also highlights the complexity of the LC's role in pain because the response to LC inhibition evolves over time and differentially across hindlimbs. One-week after SNI, the injured limb no longer responds to LC inhibition, but the non-injured limb shows enhanced sensitivity. However, four weeks after SNI, LC-mediated inhibition is restored in the injured limb with a trend towards antinociception in the non-injured limb. Following the thread of LC inhibition-mediated control of sensory thresholds, we also report that LC-MOR-mediated inhibition is critical for regulating evoked sensory thresholds. Importantly, in conditional knockout mice lacking MOR in all noradrenergic cells (*Oprm1*$^{fl/fl}$x*Dbh*$^{Cre+/-}$), we found that selectively rescuing LC-MOR signaling or the receptor itself reverses basal pronociceptive phenotypes and SNI-induced hypersensitivity, respectively (**Fig. 3 & 4**). These findings add to our understanding of the LC system in pain and suggest that strategies to maintain LC-MOR signaling may be useful for mitigating chronic pain. These results also support the hypothesis from previous literature that, despite its acute antinociceptive properties, the LC acts as a chronic pain generator(*5*, *8*, *9*, *58*). Importantly, our work also adds critical new evidence that loss of LC-MOR may underly the transition from acute analgesia system to chronic pain generator.

This additional insight into the function of LC-MOR expands this receptor system's functional role in the LC. Most prominently, LC-MOR are thought to bring an end to the LC high tonic stress

response (*25*–*30*), but important prior studies identified MOR activation in the LC as antinociceptive(*31*, *32*). Furthermore, long-term neuropathic injury causes acute MOR desensitization and reduced DAMGO responses in rats(*88*), and our results in mice suggest this inhibitory G-protein coupled system is critical for regulating LC-mediated nociception. Other contemporaneous work has identified the LC as a critical node for supraspinal exogenous opioid-mediated antinociception through the descending pain system(*89*). Altogether, these results suggest rescued mu opioid receptor function may be a therapeutic target for the treatment chronic pain. However, further study is needed to quantify MOR expression in LC neurons through the duration of neuropathic injury. It is not yet clear, however, whether MOR function is uniquely required for this effect. Previous studies have shown lesions or blockade of LC activity reverses neuropathic injury-induced hypersensitivity(*8*, *9*). Therefore, it stands to reason that other endogenous inhibitory systems within the LC may produce similar behavioral responses(*25*, *59*–*63*, *82*, *86*, *90*–*97*). Future work should pursue this hypothesis to identify new, potentially analgesic mechanisms. Further study is also needed to isolate the neural circuit underpinnings of LC-MOR-gated pain generation. One possible explanation lies in the extensive efferent circuitry of the LC-NE system(*11*). Recent elegant studies have identified discrete LC modules differentially modulating pain-related behaviors(*1*, *4*–*6*, *18*, *20*, *21*). For example, it is clear that activation of LC projections to the medial prefrontal cortex produces pronociceptive behaviors and drive hyperalgesia following neuropathic injury(*4*). It might be that LC-MOR gate the LC pain generator by selectively blunting this projection.

We report here that LC spontaneous activity is critical for normal nociception and regulation chronic nerve injury-induced hypersensitivity. These findings have broad implications for our understanding of the chronification of pain. Further study of noradrenergic circuits and inhibitory signaling pathways in these neurons will bring us closer to successfully leveraging the LC system as a target for the treatment of chronic neuropathic pain.

Materials and Methods

Animal Subjects

Adult male and female C57BL/6J (JAX:000664), *Dbh*$^{Cre+/-}$ (JAX:033951), *Oprm1*$^{fl/fl}$ (JAX: 030074), Dbh$^{Cre+/-}$ x *Oprm1*$^{fl/fl}$, and *Oprm1*$^{-/-}$ (JAX:007559) mice were used starting from age 8 weeks. Mice were originally sourced from The Jackson Laboratory (Bar Harbor, ME, USA) and bred in-house in a barrier facility in another building. These animals were transferred to a holding facility adjacent to the behavioral space between 4-6 weeks of age. Mice were then left undisturbed except for necessary husbandry to habituate to the new facility until 8 weeks of age. All mice were group-housed, given *ad libitum* access to standard laboratory chow (PicoLab Rodent Diet 20, LabDiet, St. Louis, MO, USA) and water, and maintained on a 12:12-hour light/dark cycle (lights on at 7:00 AM). All experiments and procedures were approved by the Institutional Animal Care and Use Committee of Washington University School of Medicine in accordance with National Institutes of Health guidelines.

Stereotaxic Surgery

Mice were anaesthetized in an induction chamber (3% isoflurane) and placed in a stereotaxic frame (Kopf Instruments, Model 940) where they were maintained at 1-2% isoflurane. A craniotomy was performed and mice were injected with 250 nl of AAV1-hSyn1-SIO-stGtACR2-FusionRed, AAV1-hSyn-DIO-mCherry, AAV5-syn1-FLEX-oScarlet-T2A-FLAG-hMOR-WPRE, AAV5-Ef1a-DIO-oMOR-eYFP, AAV5-Ef1a-DIO-EYFP, or AAV5-hSyn-eGFP-Cre bilaterally into the LC (stereotaxic coordinates from bregma, anterior posterior (AP): -5.45, medial lateral (ML): +/−1.10, dorsal ventral (DV): −3.75 mm. Mice were then implanted with fiber optic cannula with coordinates adjusted from viral injection -5.45 AP, +/- 1.57 ML, -3.30 DV and implanted at a 10°

angle). Implants were secured using Metabond dental cement (C&B Metabond, Edgewood, NY) and super glue. Postoperative care included carprofen tablets and subcutaneous saline injection immediately following surgery. Mice were allowed to recover for 3-6 weeks prior to behavioral testing; this interval also permitted optimal AAV expression and Cre recombinase activity. pAAV-Syn1-FLEX-mCh-T2A-FLAG-hMOR-WPRE(*79*) was a gift from Matthew Banghart (Addgene plasmid # 166970 ; http://n2t.net/addgene:166970 ; RRID:Addgene_166970) which was modified to express the oScarlet fluorophore in place of the original mCherry.

Virus Name:	Catalog #	Titer	Source
AAV1-hSyn1-SIO-stGtACR2-FusionRed	105669-AAV1	$1x10^{13}$ vg/mL	Addgene
AAV1-hSyn-DIO-mCherry	50459-AAV1	$7x10^{12}$ vg/mL	Addgene
AAV5-syn1-FLEX-oScarlet-T2A-FLAG-hMOR-WPRE	Original plasmid: Addgene# 166970	$1x10^{13}$ vg/mL	Washington University Hope Center
AAV5-Ef1a-DIO-oMOR-eYFP	N/A	$1x10^{13}$ vg/mL	Washington University Hope Center
AAV5-Ef1a-DIO-EYFP	27056-AAV5	$1x10^{13}$ vg/mL	Addgene
AAV5-hSyn-HI-eGFP-Cre-WPRE-SV40	105540-AAV5	$7x10^{12}$ vg/mL	Addgene

Stress-Induced Antinociception

Mice were immobilized in modified disposable conical tubes once for 30 minutes as previously described(*39*) and were then immediately transferred to the hot plate test.

Hot plate test

The hot plate apparatus was adapted from the operant thermal plantar assay (*98*). The hot plate was purchased from TE Technologies Inc. (CP-061HT). The Peltier device is independently controlled by a power supply (PS-12–8, 4A, TE Technology) and temperature controller (TC-48–20, TE Technology). Short cast Acrylic Tubing (7' height, E-plastics) was used to contain mice on the plate. The plate's surface temperature was monitored using a surface probe thermometer and maintained at 55°C (Pro-surface thermapen-Thermoworks). Mice were placed onto the hot plate for testing and removed either after 30 seconds of test or after completely a jump defined as both hind paws being removed from the hot plate at once.

Mechanical sensitivity (von Frey)

Mice were acclimated for 2 hours on an elevated wire mesh grid in 5-inch diameter plexiglass cylinders wrapped in black opaque plastic sheets. Mechanical hypersensitivity was determined by applying von Frey filaments (Bioseb, Pinellas Park, FL,USA) to the lateral aspect of the hind paw using the up-down method as described previously. Von Frey filaments were used at a force ranging from 0.02 g to 3.5 g. Each von Frey filament stimulation for each mouse was separated by 2 minutes. 50% withdrawal threshold was calculated as previously described.

Thermal Plantar Assay (Hargreaves)

Mice were habituated to the Hargreaves apparatus (IITC Life Science, Woodland Hills, CA) in one-hour intervals daily, three days before behavioral testing. On test day, mice were allowed to habituate for 30 minutes before testing. The heat stimulus was set to 40% intensity. Paw withdrawal was considered as the paw being removed from the Hargreaves glass surface completely before heat cessation (max duration 30 seconds). Experimental values were determined by averaging values from left and right foot except where reported separately.

Spared Nerve Injury (SNI)

The surgical procedure for the SNI-induced model of neuropathic pain was performed as described previously(*50*, *56*, *57*). Mice were anesthetized with 3% isoflurane and right hind limb shaved and disinfected with 75% ethanol and betadine. A 10-15 mm incision was made in the skin proximal to the knee to expose the biceps femoris muscle. Separation of the muscle allowed visualization of the sciatic nerve trifurcation. The common peroneal and tibial branches were ligated with 6-0 silk suture (Ethicon Inc., Raritan, NJ, USA) and 1 mm of nerve was excised distal to the ligature, leaving the sural branch intact. Following wound closure mice were allowed to recover on a table warmed to 43ºC prior to being returned to their home cage. Sham surgeries were identical to the SNI procedure without the ligation, excision, and severing of the peroneal and tibial branches of the sciatic nerve. Behavioral testing on these animals began on post-operative day 7 and wound clips were removed from the healed incision after testing was completed on post-operative day 7. Experimenters were blinded to mouse conditions including sex and injury status during experimental data collection and analysis.

Real-time place preference test

Animals were placed in a custom-made unbiased, balanced two-compartment conditioning apparatus (52.5 x 25.5 x 25.5 cm). Conditioning apparatus was filled with the same bedding used in mouse home cages equally on both sides. Mice were allowed to freely roam the entire apparatus for 20 min. Entry into one compartment triggered photostimulation of 20 Hz frequency, 2-3mW output for opto-MOR experiments and constant photostimulation, 10 mW output for GtACR2 experiments for the duration the animal remained in the light-paired chamber. Entry into the no light-paired chamber ended photostimulation.

Immunohistochemistry

Mice were anesthetized with ketamine and transcardially perfused with ice-cold 4% paraformaldehyde in 1x phosphate buffer saline (PBS). Brains were dissected, post-fixed for 24 hours at 4 ºC and cryoprotected with solution of 30% sucrose in 0.1M PB at 4ºC for at least 24 hours, cut into 30 µm sections and processed for immunostaining. 30 µm brain sections were washed three times in PBS and blocked in PBS containing 0.5% Triton X-100 and 5% normal goat serum. Sections were then incubated for ~16 hours at 4ºC in chicken anti-TH (1:1000, Aves Labs). Following incubation, sections were washed three times in PBS and then incubated for 2 hr at room temperature in Alexa Fluor 488 goat anti-chicken IgG (1:1000, Invitrogen), or Alexa Fluor 594 goat anti-chicken IgG (1:1000, Invitrogen) and then washed three times in PBS followed by three 10-min rinses in PB. Sections were then mounted on glass slides with Vectashield Antifade Mounting Medium (Vector Labs) for microscopy. All sections were imaged on an epifluorescent microscope.

Antibody name	Host Species	Target	Catalog	Dilution	Source
Anti-TH	Chicken	Tyrosine Hydroxylase	TYH	1:1000	Aves Labs Inc.
Goat anti-Chicken 488	Goat	Chicken	A11039	1:1000	Invitrogen
Goat anti-Chicken 594	Goat	Chicken	A11042	1:1000	Invitrogen

In situ hybridization

Following rapid decapitation of C57BL6/J mice, brains were rapidly frozen on dry ice. Tissue sections contained the locus coeruleus were cut at 10 µM at –20ºC and thaw-mounted onto Super

Frost Plus slides (Fisher, Waltham, MA). Slides were stored at –80ºC overnight. Fluorescent *in situ* hybridization (ISH) was performed according to the RNAScope 2.0 Fluorescent Multiple Kit User Manual for Fresh Frozen Tissue (Advanced Cell Diagnostics, Inc.), as described (*99*). Briefly, sections were fixed in 4% PFA, dehydrated with alcohol (50%, 75%, 100%) concentrations in ascending order. Sections were pretreated with hydrogen peroxide for 15 min at room temperature and washed in a 1X PBS solution twice for 2 min each. Post-wash, the sections were pretreated with protease IV solution. Sections were then incubated target probes for mouse *oprm1* (468568) (C1), *dbh (*464621) (C2). Probes were obtained from Advanced Cell Diagnostics. Following probe hybridization, sections underwent a series of probe signal amplification steps followed by incubation with fluorescently labeled probes designed to target the specified channel associated with *oprm1* (fluorescein), *dbh* (cyanin3). Slides were counterstained with DAPI, and coverslips were mounted with Vectashield Hard Set mounting medium (Vector Laboratories).

Electrophysiology

Adult mice were deeply anaesthetized via i.p. injections of a ketamine/xylazine/acepromazine cocktail. Upon sedation, mice were perfused with slicing-aCSF consisting of 92 mM N-methyl-d-glucose (NMDG), 2.5 mM KCl, 1.25 mM NaH_2PO_4, 10 mM $MgSO_4$, 20 mM HEPES, 30 mM $NaHCO_3$, 25 mM glucose, 0.5 mM $CaCl_2$, 5 mM sodium ascorbate and 3 mM sodium pyruvate, oxygenated with 95% O2 and 5% CO2. pH of aCSF solution was 7.3–7.4 and osmolality adjusted to 315–320 mOsm with sucrose. The brainstem was dissected and embedded with 2% agarose in slice-aCSF. Coronal brain slices were cut into 350µm slices using a vibratome (VF310-0Z, Precisionary Instruments, MA, USA) and incubated in warm (32°C) slicing-aCSF for 30 mins. After incubation slices were transferred to holding-aCSF containing 92 mM NaCl, 2.5 mM KCl, 1.25 mM NaH_2PO4, 30 mM $NaHCO_3$, 20 mM HEPES, 25 mM glucose, 2 mM $MgSO_4$, 2 mM $CaCl_2$, 5 mM sodium ascorbate and 3 mM sodium pyruvate, oxygenated with 95% O2 and 5% CO2. pH of solution was 7.3–7.4 and osmolality adjusted to 310–315 mOsm. Slices were placed into a recording chamber mounted on an upright microscope (BX51WI, Olympus Optical Co., Ltd, Tokyo, Japan) with epifluorescence equipment and a highspeed camera (ORCA-Flash4.0LT, Hamamatsu Photonics, Shizuoka, Japan) while perfused continuously with warm (29–31°C) recording-aCSF containing 124 mM NaCl, 2.5 mM KCl, 1.25 mM NaH_2PO_4, 24 mM $NaHCO_3$, 5 mM HEPES, 12.5 mM glucose, 2 mM $MgCl_2$, 2 mM $CaCl_2$, oxygenated with 95% O2 and 5% CO2 and pH 7.3–7.4 with osmolality adjusted to 305–310 mOsm using sucrose. All recordings were performed using visual guidance (40× water immersion objective lens, LUMPLFLN-40xW, Olympus, Tokyo, Japan) through glass pipette pulled from borosilicate glass capillary (GC150F-10, Warner Instruments, Hamden, CT, USA) with a resistance around 6-9 MΩ. For whole-cell recording, glass pipettes were filled with potassium gluconate-based intra-pipette solution consisting of 120 mM potassium gluconate, 5 mM NaCl, 10 mM HEPES, 1.1 mM EGTA, 15 mM Phosphocreatine, 2 mM ATP and 0.3 mM GTP, pH 7.2–7.3 and osmolality adjusted to 300 mOsm. Data from current-clamp mode were discarded if the membrane potential (Vm) of recorded cell was over −40 mV or action potentials did not overshoot 0 mV. For voltage-clamp recordings, membrane potential was clamped at -70mV and data was only accepted if serial resistance varied smaller than 20% of the baseline value, which was less than 20 MΩ typically. All data were collected using a Multiclamp 700B amplifier (Molecular Devices, San Jose, CA, USA) with a low-pass filtered at 2 kHz and digitized at 10k Hz through Axon Digidata 1440A interface (Molecular Devices, CA, USA) running Clampex software (Molecular Devices, CA, USA). In optogenetic experiments, brain slices were cut from *Dbh*^{Cre} mice bilaterally injected with AAV1-hSyn1-SIO-stGtACR2-FusionRed (Addgene, MA, USA) into the LC and allowed to recover for 5-8 weeks. Blue light pulses were generated from an LED light source delivered through the epifluorescence optical path controlled by Axon Digidata 1440A, light intensity was set to 10mW with 2ms duration at 0.05Hz unless specified otherwise.

For input-output relationship and input resistance data, all recordings were performed with synaptic blockers containing 200μM kynurenic acid, 1μM strychnine and 100μM picrotoxin. Recorded cells were continuously clamped at -70mV under current-clamp mode and received one second current injections with 10pA steps. Input resistance was calculated using the linear portion of responses from current injection between -30-0 pA. For pharmacology experiments shown in Fig. 5, *Oprm1*$^{fl/fl}$x*Dbh*$^{Cre+/-}$ mice were bilaterally injected with AAV5-syn1-FLEX-oScarlet-T2A-FLAG-hMOR-WPRE into the LC. Cells were recorded using the cell-attached recording method with pipettes filled with recording-aCSF. Drugs were delivered through the recording-aCSF perfusion system. Electrophysiology data were exported through Clampex software and analyzed using Matlab (MathWorks, MA, USA) and GraphPad Prism9 (GraphPad Software, MA, USA).

Statistics and data analysis

All data are expressed as mean ± SEM. In data that were normally distributed, differences between groups were determined using independent t-tests or one-way ANOVA, or two-way ANOVAs followed by post hoc comparisons if the main effect was significant at $p < 0.05$. In cases where data failed the D'Agostino and Pearson omnibus normality test or was ordinal by nature, non-parametric analyses were used. Statistical analyses were conducted using Prism 9.0 (GraphPad).

Acknowledgements

We thank the other members of the Al-Hasani and McCall labs for helpful feedback on this project. Special thanks to Patricia Jensen for the *Dbh*^{Cre} mice, Bryan A. Copits for feedback on mouse breeding strategies, and to Daniel C. Castro for the OMOR and hMOR viruses. This work was financially supported by the National Institutes of Health (R01NS117899, J.G.M.; F31NS124301, M.R.N.), the McDonnell Center for Systems Neuroscience (J.G.M.), a Collaboration Support initiative for Translational Anesthesiology Research (COSTAR) award from the Department of Anesthesiology at Washington University School of Medicine (J.G.M.), and the Rita Allen Foundation (J.G.M.) with added financial help from the Open Philanthropy Project (J.G.M.). We would like to acknowledge biorender.com for figure cartoons, the Washington University School of Medicine Hope Center for Neurological Disorders viral vector core, and the Osage Nation, Missouria, Illinois Confederacy, and many other tribes as the ancestral, traditional, and contemporary custodians of the land where this work was conducted.

Author contributions

M.R.N and J.G.M conceived the project and designed the detailed experimental protocols. M.R.N., C.-C.K., J.R.K., S.S.D., G.B., and L.V.T. performed the mouse experiments M.R.N., C.-C.K., J.R.K., S.S.D., G.B., and L.V.T., and J.G.M performed the investigation and analyzed the data. M.R.N., J.R.K., and J.G.M wrote the paper. M.R.N., J.R.K., and J.G.M edited the paper. M.R.N. and J.G.M acquired funding. J.G.M. provided research supervision. J.G.M. led overall project administration. All authors discussed the results and contributed to revision of the manuscript.

Conflict of Interest

The authors declare no conflicts of interest.

References

1. L. Hickey, Y. Li, S. J. Fyson, T. C. Watson, R. Perrins, J. Hewinson, A. G. Teschemacher, H. Furue, B. M. Lumb, A. E. Pickering, Optoactivation of locus ceruleus neurons evokes bidirectional changes in thermal nociception in rats. *J. Neurosci.* **34**, 4148–4160 (2014).

2. G. M. Tyce, T. L. Yaksh, Monoamine release from cat spinal cord by somatic stimuli: an intrinsic modulatory system. *The Journal of Physiology* **314**, 513–529 (1981).

3. H. Baba, Norepinephrine Facilitates Inhibitory Transmission in Substantia Gehtinosa of Adult Rat Spinal Cord (Part 1). **92**, 12 (2000).

4. S. Hirschberg, Y. Li, A. Randall, E. J. Kremer, A. E. Pickering, Functional dichotomy in spinal- vs prefrontal-projecting locus coeruleus modules splits descending noradrenergic analgesia from ascending aversion and anxiety in rats. *eLife Sciences* **6**, e29808 (2017).

5. M. W. Kucharczyk, F. Di Domenico, K. Bannister, Distinct brainstem to spinal cord noradrenergic pathways inversely regulate spinal neuronal activity. *Brain* **145**, 2293–2300 (2022).

6. M. W. Kucharczyk, F. Di Domenico, K. Bannister, A critical brainstem relay for mediation of diffuse noxious inhibitory controls. *Brain* **146**, 2259–2267 (2023).

7. J. C. W. Brooks, W.-E. Davies, A. E. Pickering, Resolving the Brainstem Contributions to Attentional Analgesia. *J Neurosci* **37**, 2279–2291 (2017).

8. J. J. Brightwell, B. K. Taylor, Noradrenergic neurons in the locus coeruleus contribute to neuropathic pain. *Neuroscience* **160**, 174–185 (2009).

9. R. Kaushal, B. K. Taylor, A. B. Jamal, L. Zhang, F. Ma, R. Donahue, K. N. Westlund, GABA-A receptor activity in the noradrenergic locus coeruleus drives trigeminal neuropathic pain in the rat; contribution of NAα1 receptors in the medial prefrontal cortex. *Neuroscience* **334**, 148–159 (2016).

10. C. Alba-Delgado, J. A. Mico, E. Berrocoso, Neuropathic pain increases spontaneous and noxious-evoked activity of locus coeruleus neurons. *Progress in Neuro-Psychopharmacology and Biological Psychiatry* **105**, 110121 (2021).

11. D. J. Chandler, P. Jensen, J. G. McCall, A. E. Pickering, L. A. Schwarz, N. K. Totah, Redefining Noradrenergic Neuromodulation of Behavior: Impacts of a Modular Locus Coeruleus Architecture. *J. Neurosci.* **39**, 8239–8249 (2019).

12. S. D. Robertson, N. W. Plummer, P. Jensen, Uncovering diversity in the development of central noradrenergic neurons and their efferents. *Brain Res.*, doi: 10.1016/j.brainres.2015.11.023 (2015).

13. V. A. Alvarez, C. C. Chow, E. J. Van Bockstaele, J. T. Williams, Frequency-dependent synchrony in locus ceruleus: role of electrotonic coupling. *Proc. Natl. Acad. Sci. U.S.A.* **99**, 4032–4036 (2002).

14. J. G. McCall, E. R. Siuda, D. L. Bhatti, L. A. Lawson, Z. A. McElligott, G. D. Stuber, M. R. Bruchas, Locus coeruleus to basolateral amygdala noradrenergic projections promote anxiety-like behavior. *eLife Sciences* **6**, e18247 (2017).

15. A. Uematsu, B. Z. Tan, E. A. Ycu, J. S. Cuevas, J. Koivumaa, F. Junyent, E. J. Kremer, I. B. Witten, K. Deisseroth, J. P. Johansen, Modular organization of the brainstem noradrenaline system coordinates opposing learning states. *Nat. Neurosci.* **20**, 1602–1611 (2017).

16. L. Li, X. Feng, Z. Zhou, H. Zhang, Q. Shi, Z. Lei, P. Shen, Q. Yang, B. Zhao, S. Chen, L. Li, Y. Zhang, P. Wen, Z. Lu, X. Li, F. Xu, L. Wang, Stress Accelerates Defensive Responses to Looming in Mice and Involves a Locus Coeruleus-Superior Colliculus Projection. *Curr. Biol.* **28**, 859-871.e5 (2018).

17. N. K. Totah, R. M. Neves, S. Panzeri, N. K. Logothetis, O. Eschenko, The Locus Coeruleus Is a Complex and Differentiated Neuromodulatory System. *Neuron* **99**, 1055-1068.e6 (2018).

18. C. Camarena-Delgado, M. Llorca-Torralba, I. Suárez-Pereira, L. Bravo, C. López-Martín, J. A. Garcia-Partida, J. A. Mico, E. Berrocoso, Nerve injury induces transient locus coeruleus activation over time: role of the locus coeruleus–dorsal reticular nucleus pathway. *PAIN* **163**, 943–954 (2022).

19. A. Cardenas, J. Caniglia, D. Keljalic, E. Dimitrov, Sex differences in the development of anxiodepressive-like behavior of mice subjected to sciatic nerve cuffing. *PAIN* **161**, 1861–1871 (2020).

20. M. Llorca-Torralba, C. Camarena-Delgado, I. Suárez-Pereira, L. Bravo, P. Mariscal, J. A. Garcia-Partida, C. López-Martín, H. Wei, A. Pertovaara, J. A. Mico, E. Berrocoso, Pain and depression comorbidity causes asymmetric plasticity in the locus coeruleus neurons. *Brain* **145**, 154–167 (2022).

21. M. Llorca-Torralba, I. Suárez-Pereira, L. Bravo, C. Camarena-Delgado, J. A. Garcia-Partida, J. A. Mico, E. Berrocoso, Chemogenetic Silencing of the Locus Coeruleus–Basolateral Amygdala Pathway Abolishes Pain-Induced Anxiety and Enhanced Aversive Learning in Rats. *Biological Psychiatry* **85**, 1021–1035 (2019).

22. M. Andreoli, T. Marketkar, E. Dimitrov, Contribution of amygdala CRF neurons to chronic pain. *Exp Neurol* **298**, 1–12 (2017).

23. T. Paretkar, E. Dimitrov, Activation of enkephalinergic (Enk) interneurons in the central amygdala (CeA) buffers the behavioral effects of persistent pain. *Neurobiol Dis* **124**, 364–372 (2019).

24. Properties and modulation of excitatory inputs to the locus coeruleus - Barcomb - 2022 - The Journal of Physiology - Wiley Online Library. https://physoc.onlinelibrary.wiley.com/doi/full/10.1113/JP283605?af=R.

25. a L. Curtis, N. T. Bello, R. J. Valentino, Evidence for functional release of endogenous opioids in the locus ceruleus during stress termination. *The Journal of neuroscience : the official journal of the Society for Neuroscience* **21**, RC152 (2001).

26. N. N. Chaijale, A. L. Curtis, S. K. Wood, X.-Y. Zhang, S. Bhatnagar, B. A. Reyes, E. J. Van Bockstaele, R. J. Valentino, Social stress engages opioid regulation of locus coeruleus norepinephrine neurons and induces a state of cellular and physical opiate dependence. *Neuropsychopharmacology* **38**, 1833–1843 (2013).

27. E. J. Van Bockstaele, B. A. S. Reyes, R. J. Valentino, The locus coeruleus: A key nucleus where stress and opioids intersect to mediate vulnerability to opiate abuse. *Brain Res.* **1314**, 162–174 (2010).

28. S. I. Tjoumakaris, C. Rudoy, J. Peoples, R. J. Valentino, E. J. Van Bockstaele, Cellular interactions between axon terminals containing endogenous opioid peptides or corticotropin-releasing factor in the rat locus coeruleus and surrounding dorsal pontine tegmentum. *J Comp Neurol* **466**, 445–456 (2003).

29. R. J. Valentino, E. Van Bockstaele, Opposing regulation of the locus coeruleus by corticotropin-releasing factor and opioids. Potential for reciprocal interactions between stress and opioid sensitivity. *Psychopharmacology (Berl.)* **158**, 331–342 (2001).

30. A. L. Curtis, S. C. Leiser, K. Snyder, R. J. Valentino, Predator stress engages corticotropin-releasing factor and opioid systems to alter the operating mode of locus coeruleus norepinephrine neurons. *Neuropharmacology* **62**, 1737–45 (2012).

31. S. Mohammad Ahmadi Soleimani, H. Azizi, J. Mirnajafi-Zadeh, S. Semnanian, Orexin type 1 receptor antagonism in rat locus coeruleus prevents the analgesic effect of intra-LC met-enkephalin microinjection. *Pharmacology Biochemistry and Behavior* **136**, 102–106 (2015).

32. A. C. Jongeling, M. E. Johns, A. Z. Murphy, D. L. Hammond, Persistent Inflammatory Pain Decreases the Antinociceptive Effects of the Mu Opioid Receptor Agonist DAMGO in the Locus Coeruleus of Male Rats. *Neuropharmacology* **56**, 1017–1026 (2009).

33. M. Llorca-Torralba, F. Pilar-Cuéllar, G. da Silva Borges, J. A. Mico, E. Berrocoso, Opioid receptors mRNAs expression and opioids agonist-dependent G-protein activation in the rat brain following neuropathy. *Progress in Neuro-Psychopharmacology and Biological Psychiatry* **99**, 109857 (2020).

34. S. L. Foote, G. Aston-Jones, F. E. Bloom, Impulse activity of locus coeruleus neurons in awake rats and monkeys is a function of sensory stimulation and arousal. *Proc Natl Acad Sci U S A* **77**, 3033–3037 (1980).

35. M. E. Carter, O. Yizhar, S. Chikahisa, H. Nguyen, A. Adamantidis, S. Nishino, K. Deisseroth, L. de Lecea, Tuning arousal with optogenetic modulation of locus coeruleus neurons. *Nature Neuroscience* **13**, 1526–1533 (2010).

36. G. Aston-Jones, J. Rajkowski, P. Kubiak, T. Alexinsky, Locus coeruleus neurons in monkey are selectively activated by attended cues in a vigilance task. *J. Neurosci.* **14**, 4467–4480 (1994).

37. M. G. Feenstra, M. Vogel, M. H. Botterblom, R. N. Joosten, J. P. de Bruin, Dopamine and noradrenaline efflux in the rat prefrontal cortex after classical aversive conditioning to an auditory cue. *Eur. J. Neurosci* **13**, 1051–1054 (2001).

38. S. Bouret, A. Duvel, S. Onat, S. J. Sara, Phasic activation of locus ceruleus neurons by the central nucleus of the amygdala. *J. Neurosci.* **23**, 3491–3497 (2003).

39. J. G. McCall, R. Al-Hasani, E. R. Siuda, D. Y. Hong, A. J. Norris, C. P. Ford, M. R. Bruchas, CRH Engagement of the Locus Coeruleus Noradrenergic System Mediates Stress-Induced Anxiety. *Neuron* **87**, 605–620 (2015).

40. N. R. Sciolino, N. W. Plummer, Y.-W. Chen, G. M. Alexander, S. D. Robertson, S. M. Dudek, Z. A. McElligott, P. Jensen, Recombinase-Dependent Mouse Lines for Chemogenetic Activation of Genetically Defined Cell Types. *Cell Reports* **15**, 2563–2573 (2016).

41. R. P. Tillage, S. L. Foster, D. Lustberg, L. C. Liles, K. E. McCann, D. Weinshenker, Co-released norepinephrine and galanin act on different timescales to promote stress-induced anxiety-like behavior. *Neuropsychopharmacol.* **46**, 1535–1543 (2021).

42. V. Zerbi, A. Floriou-Servou, M. Markicevic, Y. Vermeiren, O. Sturman, M. Privitera, L. von Ziegler, K. D. Ferrari, B. Weber, P. P. D. Deyn, N. Wenderoth, J. Bohacek, Rapid Reconfiguration of the Functional Connectome after Chemogenetic Locus Coeruleus Activation. *Neuron* **0** (2019).

43. H. Hayat, N. Regev, N. Matosevich, A. Sales, E. Paredes-Rodriguez, A. J. Krom, L. Bergman, Y. Li, M. Lavigne, E. J. Kremer, O. Yizhar, A. E. Pickering, Y. Nir, Locus coeruleus norepinephrine activity mediates sensory-evoked awakenings from sleep. *Science Advances* **6**, eaaz4232 (2020).

44. D. Sugiyama, S. W. Hur, A. E. Pickering, D. Kase, S. J. Kim, M. Kawamata, K. Imoto, H. Furue, In vivo patch-clamp recording from locus coeruleus neurones in the rat brainstem. *The Journal of Physiology* **590**, 2225–2231 (2012).

45. M. Mahn, L. Gibor, P. Patil, K. C.-K. Malina, S. Oring, Y. Printz, R. Levy, I. Lampl, O. Yizhar, High-efficiency optogenetic silencing with soma-targeted anion-conducting channelrhodopsins. *Nat Commun* **9**, 1–15 (2018).

46. R. N. Hughes, K. I. Bakhurin, E. A. Petter, G. D. R. Watson, N. Kim, A. D. Friedman, H. H. Yin, Ventral Tegmental Dopamine Neurons Control the Impulse Vector during Motivated Behavior. *Curr Biol* **30**, 2681-2694.e5 (2020).

47. J. E. Messier, H. Chen, Z.-L. Cai, M. Xue, Targeting light-gated chloride channels to neuronal somatodendritic domain reduces their excitatory effect in the axon. *eLife* **7**, e38506 (2018).

48. S. D. Shields, W. A. Eckert, A. I. Basbaum, Spared Nerve Injury Model of Neuropathic Pain in the Mouse: A Behavioral and Anatomic Analysis. *Journal of Pain* **4**, 465–470 (2003).

49. I. Decosterd, C. J. Woolf, Spared nerve injury: an animal model of persistent peripheral neuropathic pain. *Pain* **87**, 149–158 (2000).

50. J. Cichon, L. Sun, G. Yang, Spared Nerve Injury Model of Neuropathic Pain in Mice. *Bio-Protocol* **8**, 1–7 (2018).

51. K. E. Inyang, T. Szabo-Pardi, E. Wentworth, T. A. McDougal, G. Dussor, M. D. Burton, T. J. Price, The antidiabetic drug metformin prevents and reverses neuropathic pain and spinal cord microglial activation in male but not female mice. *Pharmacological Research* **139**, 1–16 (2019).

52. C. Paige, I. Plasencia-Fernandez, M. Kume, M. Papalampropoulou-Tsiridou, L.-E. Lorenzo, E. T. David, L. He, G. L. Mejia, C. Driskill, F. Ferrini, A. L. Feldhaus, L. F. Garcia-Martinez, A. N. Akopian, Y. D. Koninck, G. Dussor, T. J. Price, A Female-Specific Role for Calcitonin Gene-Related Peptide (CGRP) in Rodent Pain Models. *J. Neurosci.* **42**, 1930–1944 (2022).

53. M. C. Montana, B. A. Conrardy, L. F. Cavallone, B. J. Kolber, L. K. Rao, S. C. Greco, R. W. Gereau IV, Metabotropic Glutamate Receptor 5 Antagonism with Fenobam: Examination of Analgesic Tolerance and Side Effect Profile in Mice. *Anesthesiology* **115**, 1239–1250 (2011).

54. A. J. Shepherd, D. P. Mohapatra, Pharmacological validation of voluntary gait and mechanical sensitivity assays associated with inflammatory and neuropathic pain in mice. *Neuropharmacology* **130**, 18–29 (2018).

55. A. Muralidharan, S. G. Sotocinal, J.-S. Austin, J. S. Mogil, The influence of aging and duration of nerve injury on the antiallodynic efficacy of analgesics in laboratory mice. *Pain Rep* **5**, e824 (2020).

56. M. R. Norris, J. Bilbily, L. J. Becker, G. Borges, Y. Chang, S. S. Dunn, M. K. Madasu, R. Al-Hasani, M. C. Creed, J. G. McCall, Neuropathic injury drives a generalized negative affective state in mice. *bioRxiv* (2022).

57. M. R. Norris, S. S. Dunn, B. R. Aravamuthan, J. G. McCall, Spared nerve injury causes motor phenotypes unrelated to pain in mice. bioRxiv [Preprint] (2023). https://doi.org/10.1101/2023.07.07.548155.

58. B. K. Taylor, K. N. Westlund, The noradrenergic locus coeruleus as a chronic pain generator. *Journal of Neuroscience Research* **95**, 1336–1346 (2017).

59. C. P. Bailey, D. Couch, E. Johnson, K. Griffiths, E. Kelly, G. Henderson, μ-Opioid Receptor Desensitization in Mature Rat Neurons: Lack of Interaction between DAMGO and Morphine. *J. Neurosci.* **23**, 10515–10520 (2003).

60. H. M. Guajardo, K. Snyder, A. Ho, R. J. Valentino, Sex Differences in μ-Opioid Receptor Regulation of the Rat Locus Coeruleus and Their Cognitive Consequences. *Neuropsychopharmacol* **42**, 1295–1304 (2017).

61. J. T. Williams, T. M. Egan, R. A. North, Enkephalin opens potassium channels on mammalian central neurones. *Nature* **299**, 74–77 (1982).

62. M. R. Banghart, B. L. Sabatini, Photoactivatable neuropeptides for spatiotemporally precise delivery of opioids in neural tissue. *Neuron* **73**, 249–259 (2012).

63. E. J. V. Bockstaele, E. E. O. Colago, P. Cheng, A. Moriwaki, G. R. Uhl, V. M. Pickel, Ultrastructural Evidence for Prominent Distribution of the μ-Opioid Receptor at

Extrasynaptic Sites on Noradrenergic Dendrites in the Rat Nucleus Locus Coeruleus. *J. Neurosci.* **16**, 5037–5048 (1996).

64. M. Llorca-Torralba, F. Pilar-Cuéllar, L. Bravo, C. Bruzos-Cidon, M. Torrecilla, J. A. Mico, L. Ugedo, E. Garro-Martínez, E. Berrocoso, Opioid Activity in the Locus Coeruleus Is Modulated by Chronic Neuropathic Pain. *Mol Neurobiol* **56**, 4135–4150 (2019).

65. R. Weibel, D. Reiss, L. Karchewski, O. Gardon, A. Matifas, D. Filliol, J. A. J. Becker, J. N. Wood, B. L. Kieffer, C. Gaveriaux-Ruff, Mu Opioid Receptors on Primary Afferent Nav1.8 Neurons Contribute to Opiate-Induced Analgesia: Insight from Conditional Knockout Mice. *PLoS One* **8**, e74706 (2013).

66. H. W. D. Matthes, R. Maldonado, F. Simonin, O. Valverde, S. Slowe, I. Kitchen, K. Befort, A. Dierich, M. L. Meur, P. Dollé, E. Tzavara, J. Hanoune, B. P. Roques, B. L. Kieffer, Loss of morphine-induced analgesia, reward effect and withdrawal symptoms in mice lacking the μ-opioid-receptor gene. *Nature* **383**, 819–823 (1996).

67. M. Martin, A. Matifas, R. Maldonado, B. L. Kieffer, Acute antinociceptive responses in single and combinatorial opioid receptor knockout mice: distinct mu, delta and kappa tones. *Eur J Neurosci* **17**, 701–708 (2003).

68. M. M. Heinricher, J. P. Rosenfeld, Microinjection of morphine into nucleus reticularis paragigantocellularis of the rat suppresses spontaneous activity of nucleus raphe magnus neurons. *Brain Res* **272**, 382–386 (1983).

69. A. I. Basbaum, C. H. Clanton, H. L. Fields, Opiate and stimulus-produced analgesia: functional anatomy of a medullospinal pathway. *Proc Natl Acad Sci U S A* **73**, 4685–4688 (1976).

70. H. L. Fields, S. D. Anderson, C. H. Clanton, A. I. Basbaum, Nucleus raphe magnus: a common mediator of opiate- and stimulus-produced analgesia. *Trans Am Neurol Assoc* **101**, 208–210 (1976).

71. Z. F. Cheng, H. L. Fields, M. M. Heinricher, Morphine microinjected into the periaqueductal gray has differential effects on 3 classes of medullary neurons. *Brain Res* **375**, 57–65 (1986).

72. H. L. Fields, A. I. Basbaum, Brainstem control of spinal pain-transmission neurons. *Annu Rev Physiol* **40**, 217–248 (1978).

73. G. F. Gebhart, C. L. Mitchell, The effect of adrenalectomy on morphine analgesia and tolerance development in rats. *Eur J Pharmacol* **18**, 37–42 (1972).

74. K. B. McPherson, C. A. Bouchet, B. Coutens, S. L. Ingram, Persistent inflammation selectively activates opioid-sensitive phasic-firing neurons within the vlPAG. *J Neurophysiol* **129**, 1237–1248 (2023).

75. G. Scherrer, N. Imamachi, Y.-Q. Cao, C. Contet, F. Mennicken, D. O'Donnell, B. L. Kieffer, A. I. Basbaum, Dissociation of the opioid receptor mechanisms that control mechanical and heat pain. *Cell* **137**, 1148–1159 (2009).

76. G. Corder, D. C. Castro, M. R. Bruchas, G. Scherrer, Endogenous and Exogenous Opioids in Pain. *Annu. Rev. Neurosci.*, doi: 10.1146/annurev-neuro-080317-061522 (2018).

77. F. Porreca, H. I. Mosberg, R. Hurst, V. J. Hruby, T. F. Burks, Roles of mu, delta and kappa opioid receptors in spinal and supraspinal mediation of gastrointestinal transit effects and hot-plate analgesia in the mouse. *J Pharmacol Exp Ther* **230**, 341–348 (1984).

78. E. R. Siuda, B. A. Copits, M. J. Schmidt, M. A. Baird, R. Al-Hasani, W. J. Planer, S. C. Funderburk, J. G. McCall, R. W. Gereau IV, M. R. Bruchas, Spatiotemporal Control of Opioid Signaling and Behavior. *Neuron* **86**, 923–935 (2015).

79. S. Liu, D.-I. Kim, T. G. Oh, G. M. Pao, J.-H. Kim, R. D. Palmiter, M. R. Banghart, K.-F. Lee, R. M. Evans, S. Han, Neural basis of opioid-induced respiratory depression and its rescue. *Proceedings of the National Academy of Sciences* **118**, e2022134118 (2021).

80. S. W. Hughes, L. Hickey, R. P. Hulse, B. M. Lumb, A. E. Pickering, Endogenous analgesic action of the pontospinal noradrenergic system spatially restricts and temporally delays the progression of neuropathic pain following tibial nerve injury. *Pain* **154**, 1680–1690 (2013).

81. S. Hughes, L. Hickey, L. F. Donaldson, B. M. Lumb, A. E. Pickering, Intrathecal reboxetine suppresses evoked and ongoing neuropathic pain behaviours by restoring spinal noradrenergic inhibitory tone. *Pain* **156**, 328–334 (2015).

82. K. Hayashida, H. Obata, K. Nakajima, J. C. Eisenach, Gabapentin Acts within the Locus Coeruleus to Alleviate Neuropathic Pain. *Anesthesiology* **109**, 1077–1084 (2008).

83. M. Kimura, T. Suto, J. C. Eisenach, K. Hayashida, Down-regulation of astroglial glutamate transporter-1 in the locus coeruleus impairs pain-evoked endogenous analgesia in rats. *Neurosci. Lett.* **608**, 18–22 (2015).

84. M. Kimura, J. C. Eisenach, K.-I. Hayashida, Gabapentin loses efficacy over time after nerve injury in rats: role of glutamate transporter-1 in the locus coeruleus. *Pain* **157**, 2024–2032 (2016).

85. X. Gu, Y. Z. Zhang, J. J. O'Malley, C. C. De Preter, M. Penzo, M. A. Hoon, Neurons in the caudal ventrolateral medulla mediate descending pain control. *Nat Neurosci* **26**, 594–605 (2023).

86. A. T. Luskin, L. Li, X. Fu, K. Barcomb, T. Blackburn, E. M. Li, A. Rana, R. C. Simon, L. Sun, A. D. Murry, S. A. Golden, G. D. Stuber, C. P. Ford, L. Gu, M. R. Bruchas, A diverse network of pericoerulear neurons control arousal states. bioRxiv [Preprint] (2022). https://doi.org/10.1101/2022.06.30.498327.

87. C. Alba-Delgado, M. Llorca-Torralba, I. Horrillo, J. E. Ortega, J. A. Mico, P. Sánchez-Blázquez, J. J. Meana, E. Berrocoso, Chronic pain leads to concomitant noradrenergic impairment and mood disorders. *Biological Psychiatry* **73**, 54–62 (2013).

88. M. Llorca-torralba, F. Pilar-cuéllar, L. Bravo, C. Bruzos-cidon, M. Torrecilla, Opioid Activity in the Locus Coeruleus Is Modulated by Chronic Neuropathic Pain. 4135–4150 (2019).

89. S. T. Lubejko, G. Livrizzi, J. Patel, J. Yung, T. L. Yaksh, M. R. Banghart, Inputs to the locus coeruleus from the periaqueductal gray and rostroventral medulla shape opioid-mediated descending pain modulation. bioRxiv [Preprint] (2023). https://doi.org/10.1101/2023.10.10.561768.

90. G. Aston-Jones, Y. Zhu, J. P. Card, Numerous GABAergic afferents to locus ceruleus in the pericerulear dendritic zone: possible interneuronal pool. *J. Neurosci.* **24**, 2313–2321 (2004).

91. M. Connor, C. W. Vaughan, B. Chieng, M. J. Christie, Nociceptin receptor coupling to a potassium conductance in rat locus coeruleus neurones in vitro. *Br J Pharmacol* **119**, 1614–1618 (1996).

92. T. H. Chiu, Y. R. Yang, J. J. Yang, C. L. Chen, Inhibition of locus coeruleus neurons by serotonin at high doses. *Chin J Physiol* **38**, 153–157 (1995).

93. G. K. Aghajanian, C. P. VanderMaelen, alpha 2-adrenoceptor-mediated hyperpolarization of locus coeruleus neurons: intracellular studies in vivo. *Science* **215**, 1394–1396 (1982).

94. G. K. Aghajanian, J. M. Cedarbaum, R. Y. Wang, Evidence for norepinephrine-mediated collateral inhibition of locus coeruleus neurons. *Brain Research* **136**, 570–577 (1977).

95. C.-C. Kuo, J.-C. Hsieh, H.-C. Tsai, Y.-S. Kuo, H.-J. Yau, C.-C. Chen, R.-F. Chen, H.-W. Yang, M.-Y. Min, Inhibitory interneurons regulate phasic activity of noradrenergic neurons in the mouse locus coeruleus and functional implications. *The Journal of Physiology* **598**, 4003–4029 (2020).

96. D. Riga, K. Rademakers, I. G. Wolterink-Donselaar, F. J. Meye, Neuropeptide Y neurons of the locus coeruleus inhibit noradrenergic system activity to reduce anxiety. bioRxiv [Preprint] (2023). https://doi.org/10.1101/2023.10.16.562534.

97. J. A. Tkaczynski, O. Borodovitsyna, D. J. Chandler, Delta Opioid Receptors and Enkephalinergic Signaling within Locus Coeruleus Promote Stress Resilience. *Brain Sci* **12**, 860 (2022).

98. A. N. Reker, S. Chen, K. Etter, T. Burger, M. Caudill, S. Davidson, The operant plantar thermal assay: A novel device for assessing thermal pain tolerance in mice. *eNeuro* **7** (2020).

99. F. Wang, J. Flanagan, N. Su, L. C. Wang, S. Bui, A. Nielson, X. Wu, H. T. Vo, X. J. Ma, Y. Luo, RNAscope: A novel in situ RNA analysis platform for formalin-fixed, paraffin-embedded tissues. *Journal of Molecular Diagnostics* **14**, 22–29 (2012).

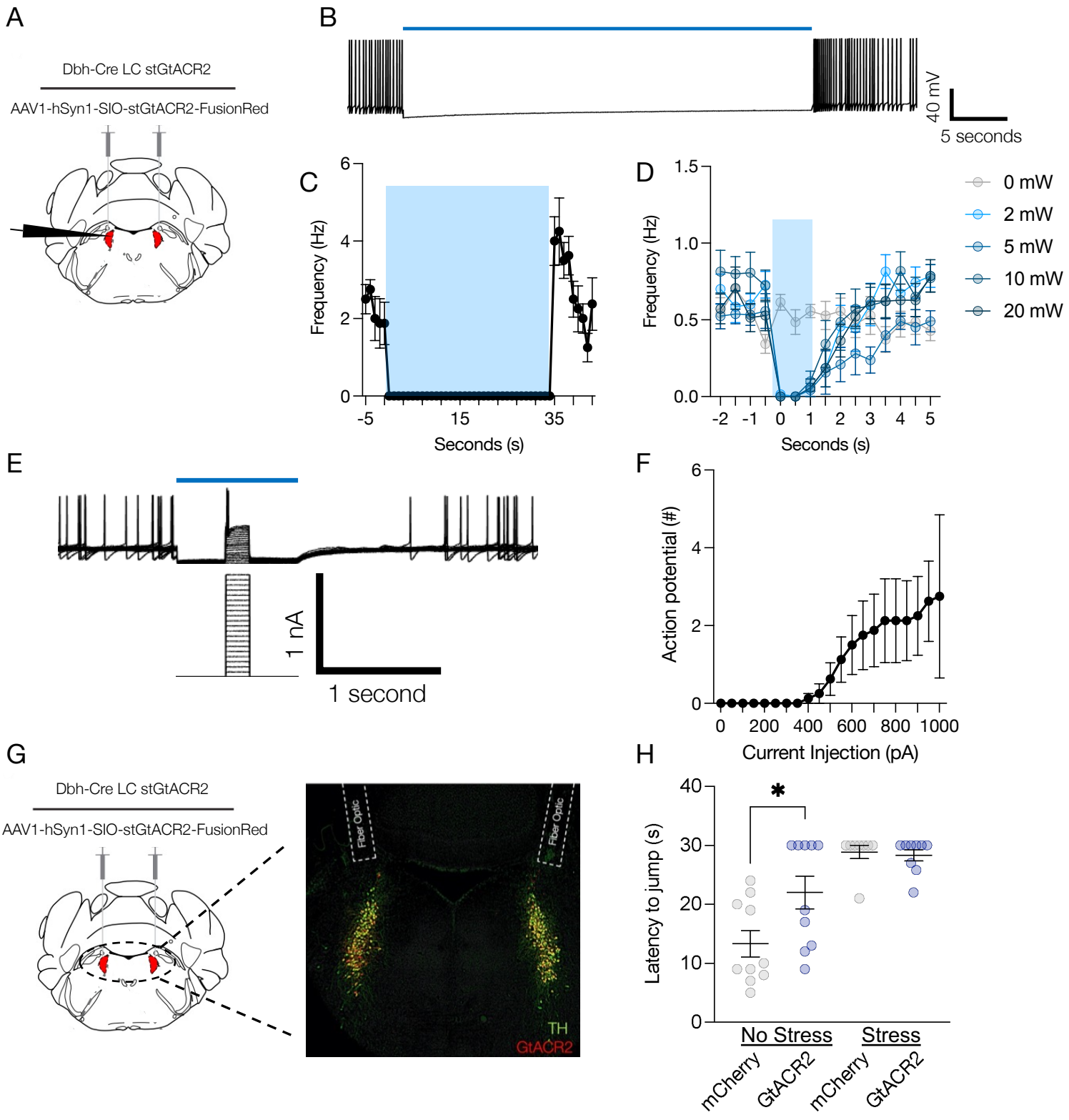
A
Dbh-Cre LC stGtACR2
AAV1-hSyn1-SIO-stGtACR2-FusionRed
B
40 mV
5 seconds
C
Frequency (Hz)
Seconds (s)
D
Frequency (Hz)
Seconds (s)
0 mW
2 mW
5 mW
10 mW
20 mW
E
1 nA
1 second
F
Action potential (#)
Current Injection (pA)
G
Dbh-Cre LC stGtACR2
AAV1-hSyn1-SIO-stGtACR2-FusionRed
Fiber Optic
Fiber Optic
TH
GtACR2
H
Latency to jump (s)
*
No Stress
Stress
mCherry
GtACR2
mCherry
GtACR2

Figure 1

Figure 1. High tonic LC activity during hot plate test is not necessary for stress-induced antinociception. (**A**) Cartoon describing viral strategy for electrophysiological validation of stGtACR2. (**B**) Whole-cell recording of locus coeruleus neuron expressing stGtACR2. (**C**) 470 nm photostimulation robustly inhibited locus coeruleus spontaneous activity. (**D**) Light power intensity response curve shows stGtACR2 is efficiently suppressed LC. (**E**) Representative whole-cell recording traces demonstrating efficacy of stGtACR2-mediated inhibition of locus coeruleus neurons against current injection. (**F**) Quantification of optical inhibition against injected current. (**G**) Cartoon of stGtACR2 viral strategy with representative immunohistochemical validation of viral expression and fiber optic placement. Tyrosine Hydroxylase=TH (green), stGtACR2-FusionRed (red). (**H**) Inhibition of LC neurons following restraint stress does not alter jump latency on a hot plate, but inhibition of LC neurons in naïve mice is antinociceptive. Data represented as mean ± SEM, n=8–13/group: One-Way ANOVA, Tukey post-hoc. No Stress mCherry vs. No Stress stGtACR2 *p=0.0192.

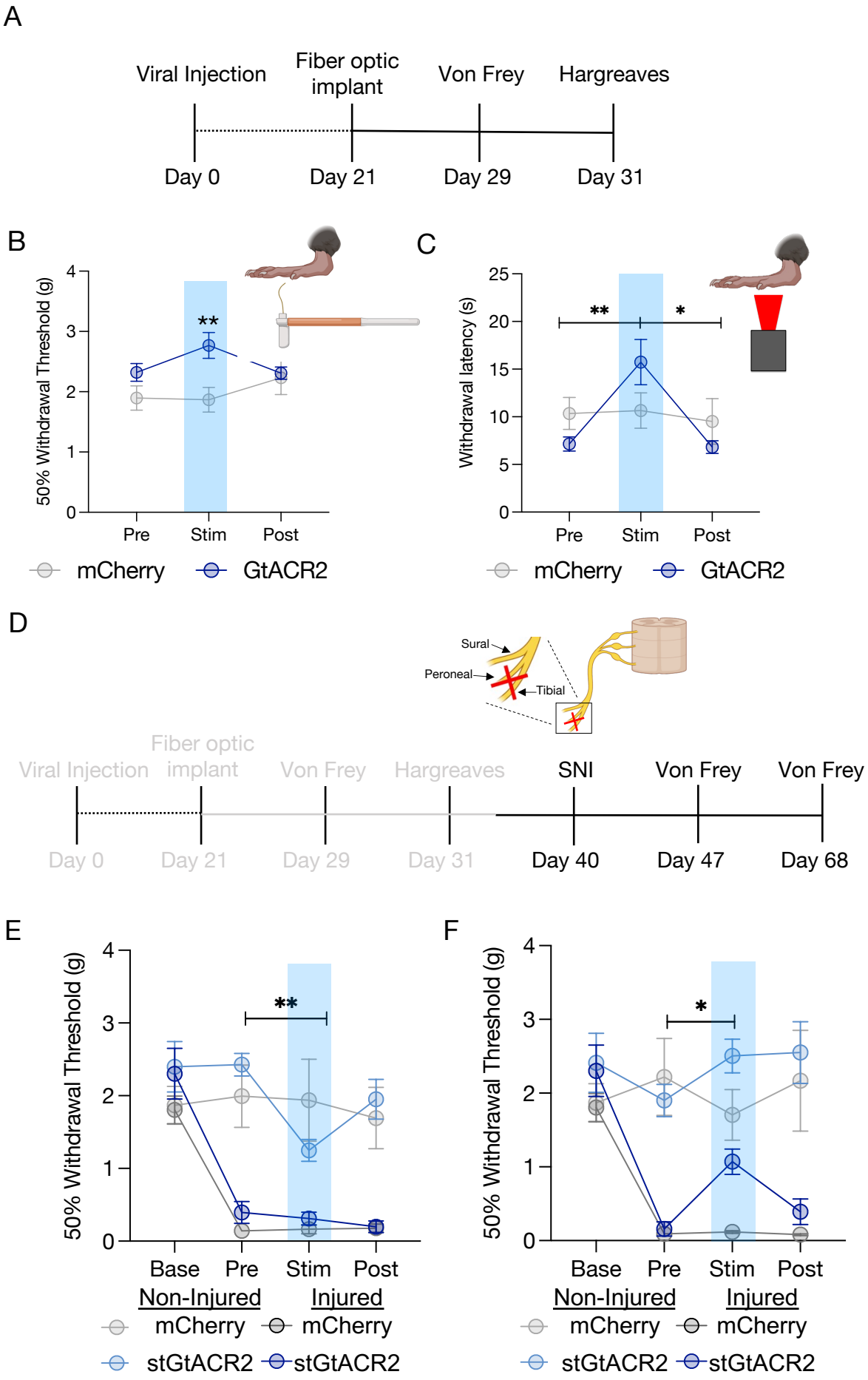
A
Viral Injection
Fiber optic implant
Von Frey
Hargreaves
Day 0
Day 21
Day 29
Day 31
B
50% Withdrawal Threshold (g)
**
Pre
Stim
Post
mCherry
GtACR2
C
Withdrawal latency (s)
**
*
Pre
Stim
Post
mCherry
GtACR2
D
Sural
Peroneal
Tibial
Viral Injection
Fiber optic implant
Von Frey
Hargreaves
SNI
Von Frey
Von Frey
Day 0
Day 21
Day 29
Day 31
Day 40
Day 47
Day 68
E
50% Withdrawal Threshold (g)
**
Base
Pre
Stim
Post
Non-Injured
Injured
mCherry
mCherry
stGtACR2
stGtACR2
F
50% Withdrawal Threshold (g)
*
Base
Pre
Stim
Post
Non-Injured
Injured
mCherry
mCherry
stGtACR2
stGtACR2

Figure 2

Figure 2. Spontaneous locus coeruleus activity contributes to baseline nociceptive thresholds. (**A**) Experimental timeline. (**B&C**) Hargreaves and von Frey results showing locus coeruleus inhibition induces antinociception. Data represented as mean +/- SEM; n=6-9/group; two-way ANOVA, Sidak's posthoc (von Frey: Time x Group $F(2,26) = 3.861$, $p=0.0340$; mCherry Stim vs. stGtACR2 Stim **$p=0.0060$; Hargreaves, stGtACR2 Stim vs. Post, mCherry stim vs. stGtACR2 stim *$p<0.05$, **$p<0.01$). (**D**) Experimental timeline with gray areas describing data shown in **A-C** and black areas describing data shown in (**E&F**). (**E**) Locus coeruleus inhibition one week after spared nerve injury is no longer antinociceptive on the injured limb, but is pronociceptive on the non-injured limb. Data represented as mean +/- SEM; n=6-9/group; two-way ANOVA ,Group x Time $F (3, 42) = 8.528$, $p=0.0002$, Tukey posthoc (stGtACR2 Non-Injured Pre vs. GtACR2 Non-Injured Stim **$p=0.0045$). (**F**) Locus coeruleus inhibition four weeks after spared nerve injury is analgesic. Data represented as mean +/- SEM; n=6-9/group; Mixed Effects Model $p=0.0003$, Tukey posthoc (stGtACR2 Injured Pre vs. GtACR2 Injured Stim *$p=0.0132$).

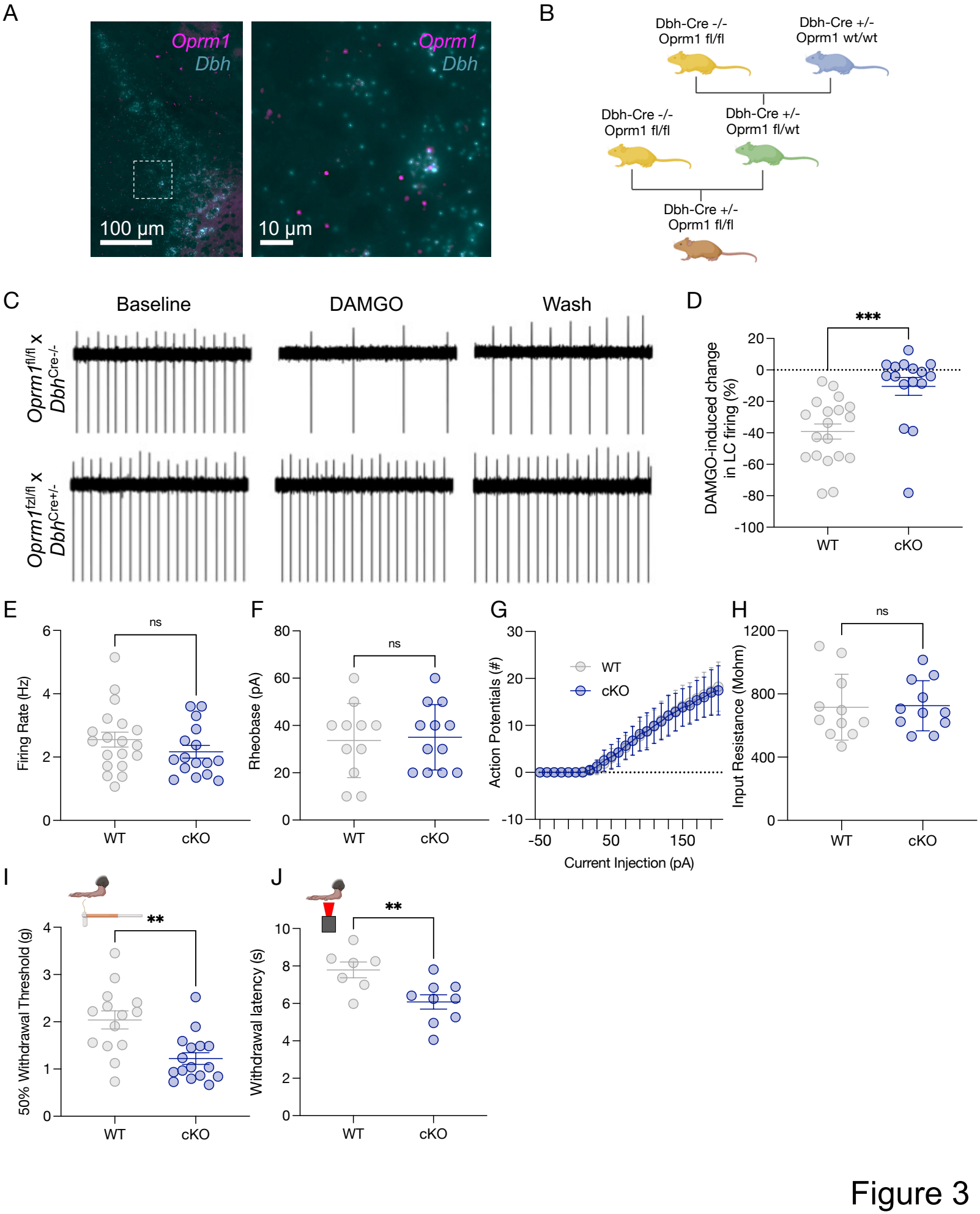
A
Oprm1
Dbh
100 µm
Oprm1
Dbh
10 µm
B
Dbh-Cre -/-
Oprm1 fl/fl
Dbh-Cre +/-
Oprm1 wt/wt
Dbh-Cre -/-
Oprm1 fl/fl
Dbh-Cre +/-
Oprm1 fl/wt
Dbh-Cre +/-
Oprm1 fl/fl
C
Baseline
DAMGO
Wash
Oprm1fl/fl x Dbh Cre-/-
Oprm1fl/fl x Dbh Cre+/-
D
***
DAMGO-induced change in LC firing (%)
20
0
-20
-40
-60
-80
-100
WT
cKO
E
ns
Firing Rate (Hz)
6
4
2
0
WT
cKO
F
ns
Rheobase (pA)
80
60
40
20
0
WT
cKO
G
WT
cKO
Action Potentials (#)
30
20
10
0
-10
-50
50
150
Current Injection (pA)
H
ns
Input Resistance (Mohm)
1200
800
400
0
WT
cKO
I
**
50% Withdrawal Threshold (g)
4
3
2
1
0
WT
cKO
J
**
Withdrawal latency (s)
10
8
6
4
2
0
WT
cKO

Figure 3

Figure 3. LC-MOR are required for noradrenergic-modulated nociception (**A**) *In situ* hybridization results of RNA colocalization of *oprm1* (purple) and *dbh* (blue). (**B**) Cartoon describing *Oprm1*$^{fl/fl}$x*Dbh*$^{Cre+/-}$ breeding strategy. (**C**) Cell-attached *ex vivo* LC recordings in *Oprm1*$^{fl/fl}$x*Dbh*$^{Cre-/-}$ (top) and *Oprm1*$^{fl/fl}$x*Dbh*$^{Cre+/-}$ (bottom) in response to DAMGO administration. (**D**) DAMGO-induced cellular inhibition of LC neurons is lost in *Oprm1*$^{fl/fl}$x*Dbh*$^{Cre+/-}$ mice. Data expressed as mean +/- SEM, n=16-19/group, unpaired parametric t-test ***p<0.001. Excitability parameters of locus coeruleus neurons between WT (*Oprm1*$^{fl/fl}$x*Dbh*$^{Cre-/-}$) and cKO (*Oprm1*$^{fl/fl}$x*Dbh*$^{Cre+/-}$) mice show no significant differences. These measures include (**E**) baseline firing rate, (**F**) rheobase, (**G**) input-output relationship of number of action potentials fired per current step, and (**H**) input resistance. Data expressed as mean +/- SEM, n=11-19/group, unpaired t-test. (**I**) von Frey test shows a significant decrease in 50% withdrawal threshold in cKO (*Oprm1*$^{fl/fl}$x*Dbh*$^{Cre+/-}$) compared to WT (*Oprm1*$^{fl/fl}$x*Dbh*$^{Cre-/-}$) control mice. Data expressed as mean +/- SEM, n=14-16/group, unpaired parametric t-test **p<0.01 (L) Baseline thermal withdrawal in Hargreaves testing is also significantly decreased in thermal withdrawal threshold in cKO (*Oprm1*$^{fl/fl}$x*Dbh*$^{Cre+/-}$) mice. Data expressed as mean +/- SEM, n=7-8/group, unpaired t-test **p<0.01.

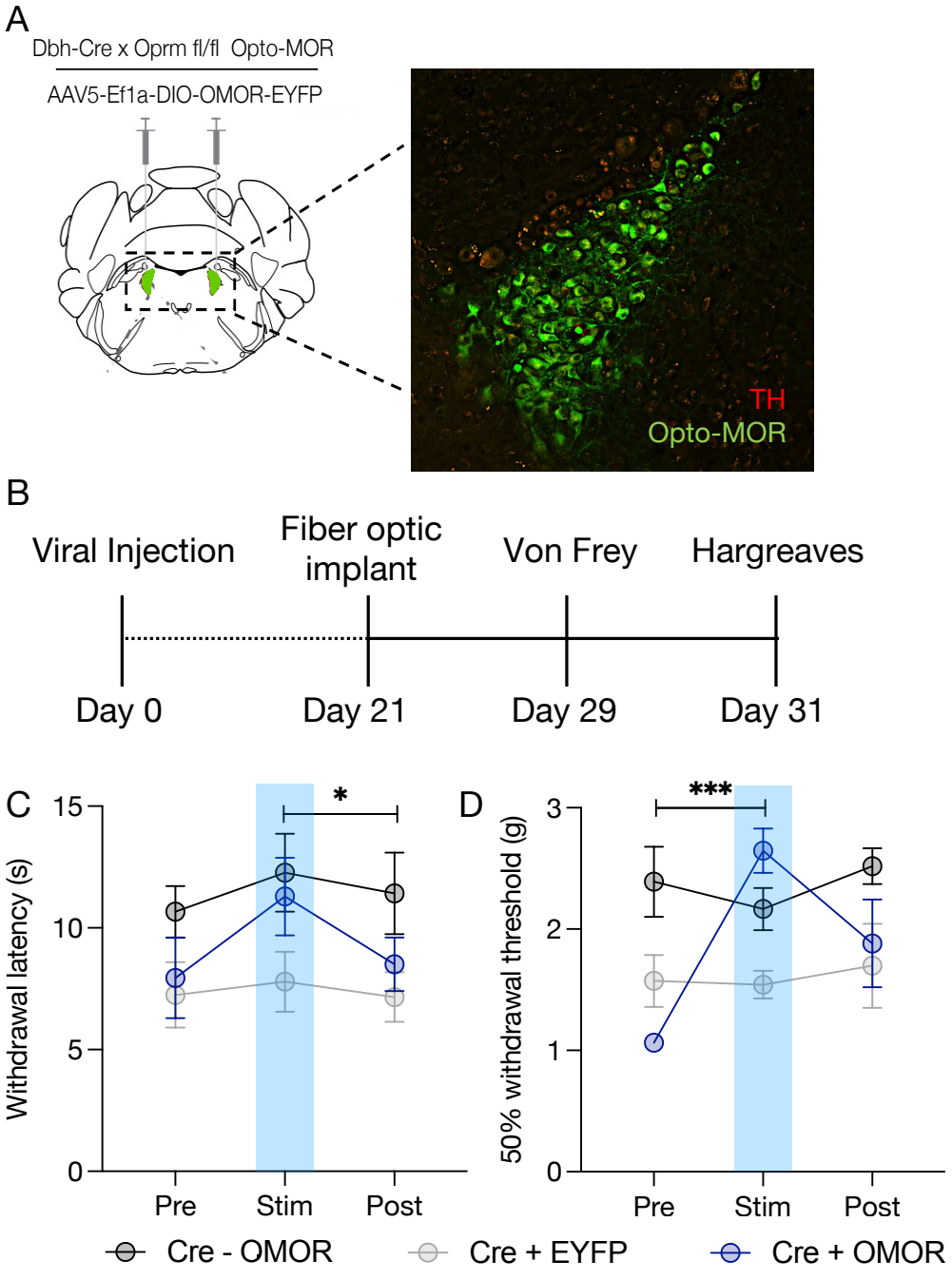
A
Dbh-Cre x Oprm fl/fl Opto-MOR
AAV5-Ef1a-DIO-OMOR-EYFP
TH
Opto-MOR
B
Viral Injection
Fiber optic implant
Von Frey
Hargreaves
Day 0
Day 21
Day 29
Day 31
C
Withdrawal latency (s)
15
10
5
0
*
Pre
Stim
Post
D
50% withdrawal threshold (g)
3
2
1
0
***
Pre
Stim
Post
Cre - OMOR
Cre + EYFP
Cre + OMOR

Figure 4

Figure 4. Restoration of LC-MOR signaling reverses baseline mechanical and thermal hypersensitivity. (**A**) Cartoon of Opto-MOR viral strategy with immunohistochemical validation of viral expression. Tyrosine Hydroxylase=TH (red), Opto-MOR-eYFP (green). (**B**) Opto-MOR experimental timeline. (**C**) opto-MOR activation in the LC restores normal thermal sensitivity in Hargreaves testing. There is a significant within subject difference between Cre+OMOR group Stim vs. Post. Data expressed as mean +/- SEM, n=7-11/group, two-way ANOVA with Tukey's multiple comparisons *$p<0.05$. (**D**) Opto-MOR activation significantly reverses baseline mechanical hypersensitivity in von Frey test. Within subject effect between Cre+OMOR Pre vs. Stim groups. Data expressed as mean +/- SEM, n=7-11/group, two-way ANOVA with Tukey's multiple comparisons ***$p<0.001$.

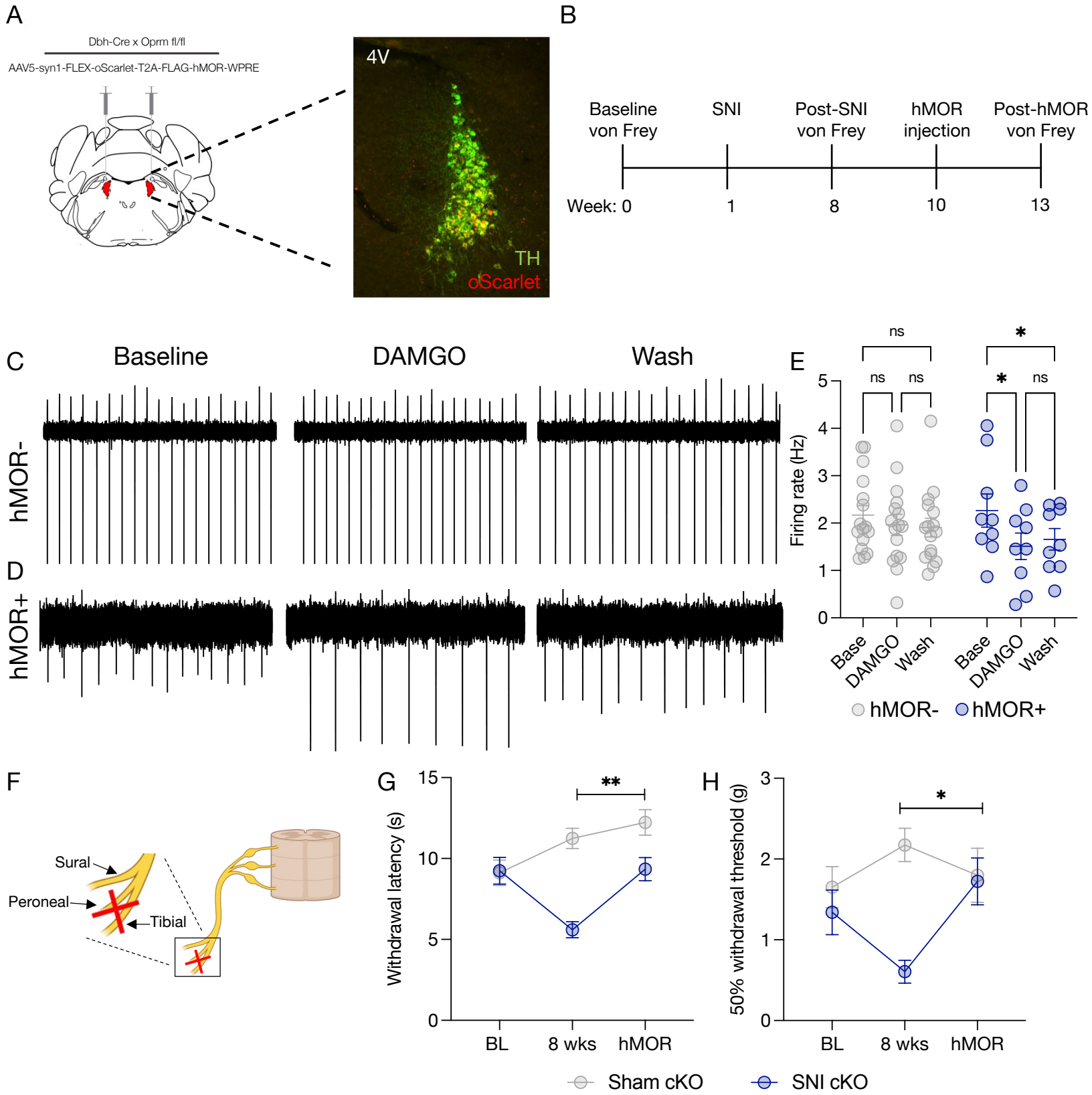
A
Dbh-Cre x Oprm fl/fl
AAV5-syn1-FLEX-oScarlet-T2A-FLAG-hMOR-WPRE
4V
TH
oScarlet
B
Baseline von Frey
SNI
Post-SNI von Frey
hMOR injection
Post-hMOR von Frey
Week: 0
1
8
10
13
C
Baseline
DAMGO
Wash
hMOR-
D
hMOR+
E
Firing rate (Hz)
ns
*
Base
DAMGO
Wash
hMOR-
hMOR+
F
Sural
Peroneal
Tibial
G
Withdrawal latency (s)
**
BL
8 wks
hMOR
Sham cKO
SNI cKO
H
50% withdrawal threshold (g)
*

Figure 5

Figure 5. LC-MOR receptor rescue reverses neuropathic injury-induced hypersensitivity (**A**) Cartoon of hMOR viral strategy with immunohistochemical validation of viral expression. Tyrosine Hydroxylase=TH (green), hMOR-expressing neurons are filled with oScarlet (red). (**B**) Experimental timeline. (**C&D**) Cell-attached *ex vivo* electrophysiology of DAMGO-mediated suppression of LC firing in *Oprm1*$^{fl/fl}$x*Dbh*$^{Cre+/-}$ mice without hMOR (**C**) and with hMOR expression (**D**). (**E**) Quantification shows significant rescue of DAMGO-induced inhibitory responses in the LC of *Oprm1*$^{fl/fl}$x*Dbh*$^{Cre+/-}$ mice with hMOR compared to those without. Data expressed as mean +/- SEM, n=9-16/group, two-way ANOVA with Tukey's multiple comparisons *p<0.05. (**F**) Cartoon describing spared nerve injury model. (**G**) Rescue of MOR expression reverses neuropathic pain-induced thermal hypersensitivity. Data expressed as mean +/- SEM, n=8-10/group, two-way ANOVA Cre+ injured paw 8 weeks vs. hMOR **p<0.01. (**H**) Rescue of MOR expression reverses neuropathic pain-induced mechanical hypersensitivity. Data expressed as mean +/- SEM, n=8-10/group, two-way ANOVA Cre+ injured paw 8 weeks vs. hMOR *p<0.05.

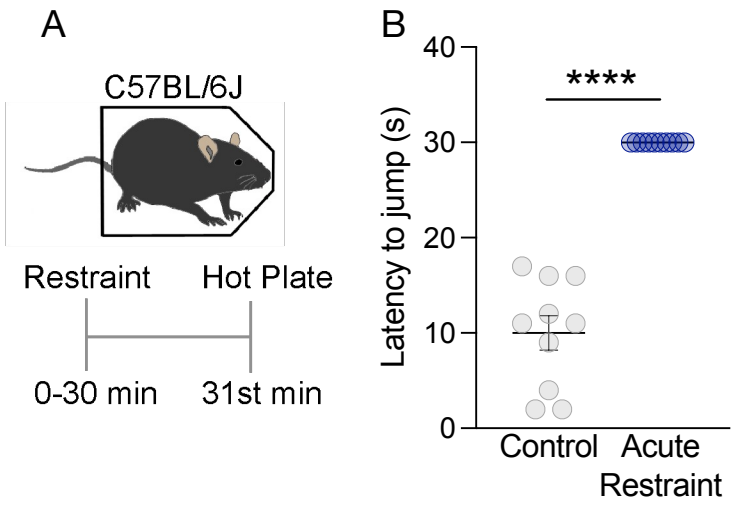

Supplementary Figure 1: Acute restraint stress causes acute antinociception. (**A**) Cartoon and experimental timeline of restraint stress-induced antinociceptive testing on the hot plate test. (**B**) 30 minutes of restraint stress drives thermal antinociception as delayed nocifensive responses on a 55ºC hot plate with 30 second cutoff. n= 10/group. Mann-Whitney test (No Stress vs. Acute Restraint) U=0, p<0.0001.

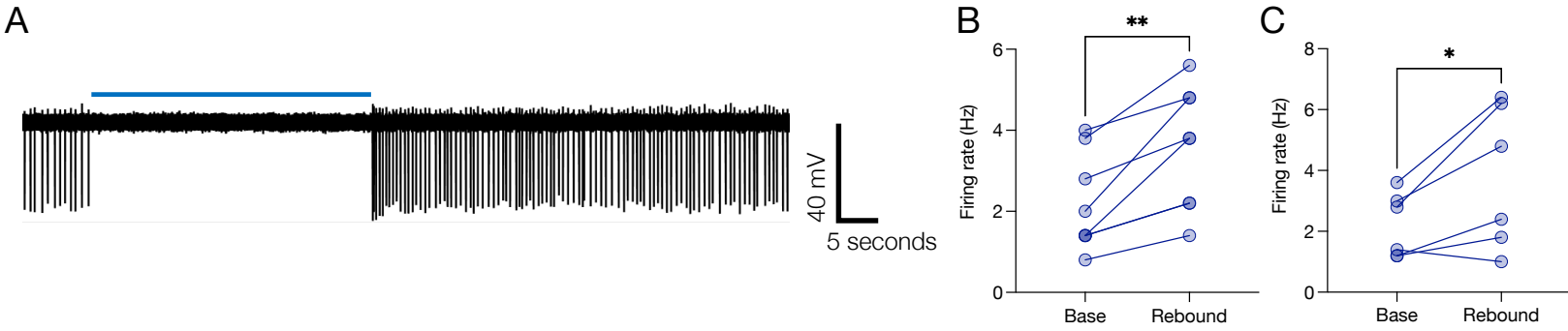

Supplemental Figure 2. stGtACR2 robustly silences LC neuronal activity (**A**) Cell-attached ex vivo recording of stGtACR2-expressing LC neuron. (**B&C**) Quantification of rebound effect of LC neuronal firing following photoinhibition in (**B**) whole-cell current clamp and (**C**) cell-attached recordings. Data expressed as mean +/- SEM, paired t-test (**B**) t=4.604, df=7, **p=0.0025 **(C**) t=2.731, df=5 *p=0.0412

Supplementary Figure 2

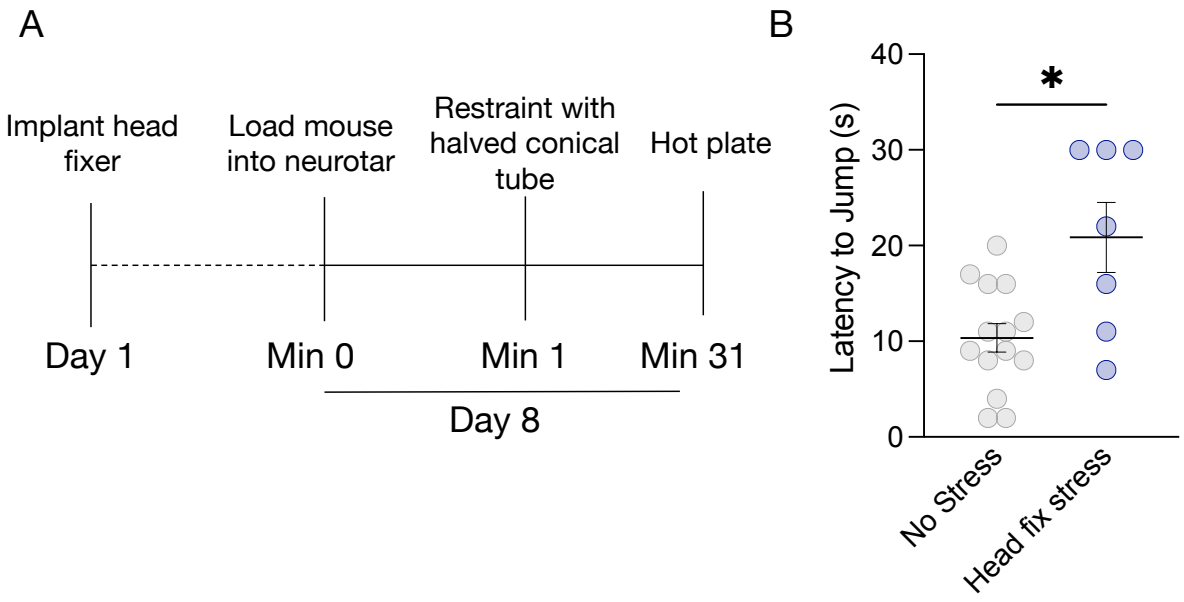

Supplementary Figure 3: Modified acute restraint stress to include head-fixation causes acute antinociception. (**A**) Experimental timeline of head-fixed restraint stress-induced antinociceptive testing on the hot plate test. (**B**) 30 minutes of head-fixed restraint stress drives thermal antinociception as delayed nocifensive responses on a 55ºC hot plate with 30 second cutoff. n= 7-14/group. Mann-Whitney test (No Stress vs, Head fix stress) U=20, *p=0.0289.

Supplementary Figure 3

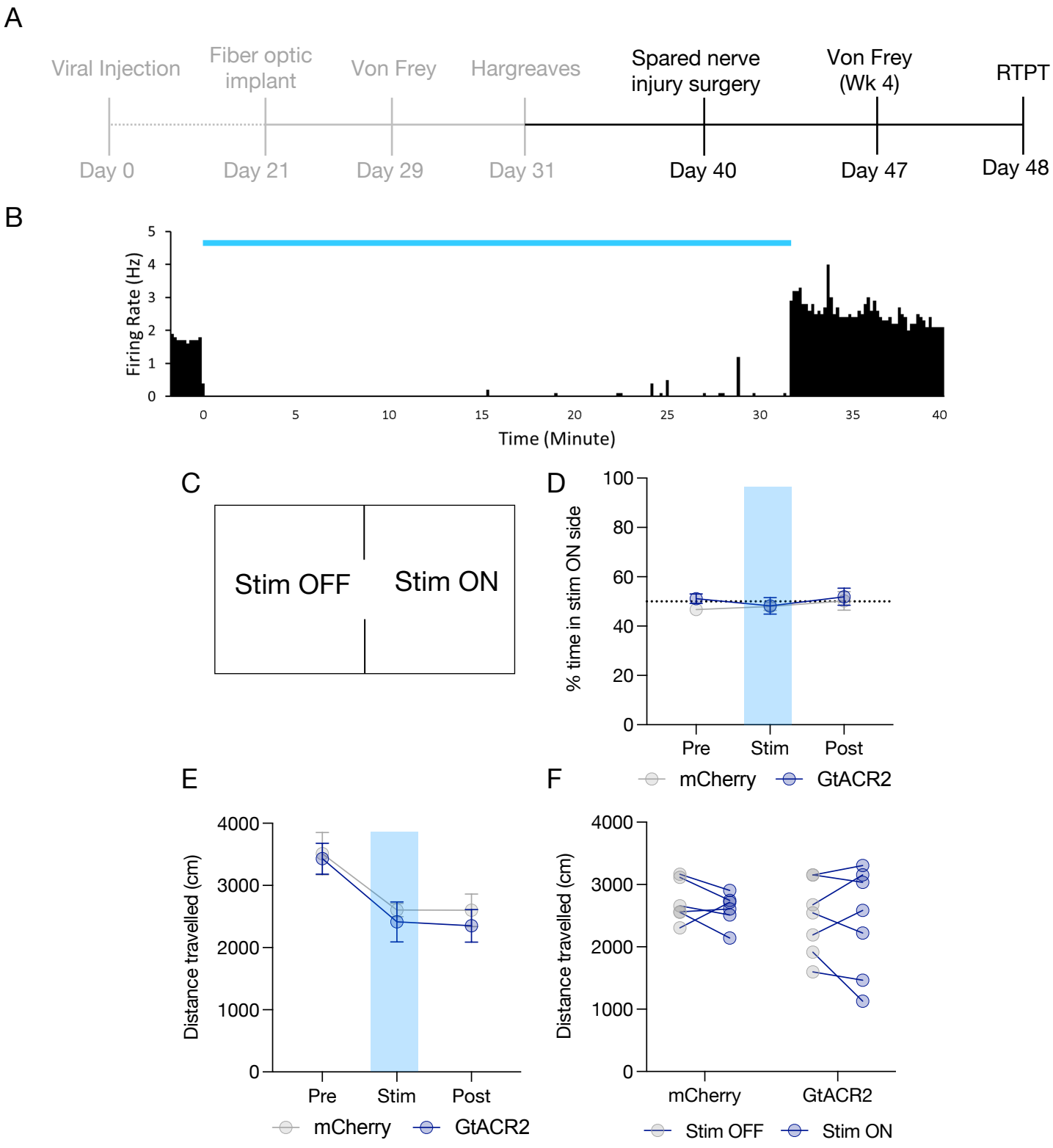

Supplement Figure 4. LC inhibition does not induce real-time preference four weeks after neuropathic injury (**A**) Experimental timeline. (**B**) Electrophysiological validation of prolonged LC inhibition using 100 Hz,0.5ms duration 470 nm stimulation for 30 minutes. (**C**) Diagram of real-time place testing setup. (**D**) LC inhibition does not induce real-time place preference four weeks post neuropathic injury. (**E&F**) LC inhibition does not alter distance travelled in real-time place test. Data expressed as mean +/- SEM.

Supplementary Figure 4

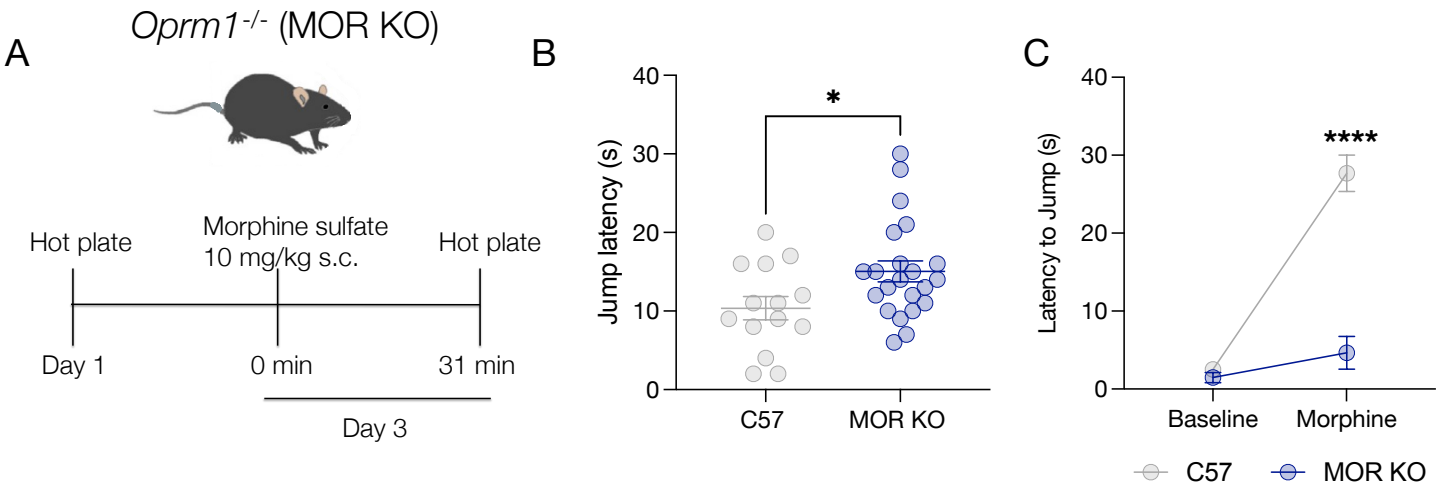

Supplement Figure 5. Global *oprm1* knockout influences nociceptive output (**A**) Experimental timeline using global *oprm1*$^{-/-}$ mice. (**B**) Naïve *oprm1*$^{-/-}$ mice have increased nociceptive threshold on a hot plate. Data expressed as mean +/- SEM, unpaired t-test, *p<0.05. (**C**) *oprm1*$^{-/-}$ mice do not have morphine analgesia. Data expressed as mean +/- SEM, 2-way ANOVA with Tukey's multiple comparisons, C57BL/6J morphine vs. *oprm1*$^{-/-}$ morphine ****p<0.0001.

Supplementary Figure 5

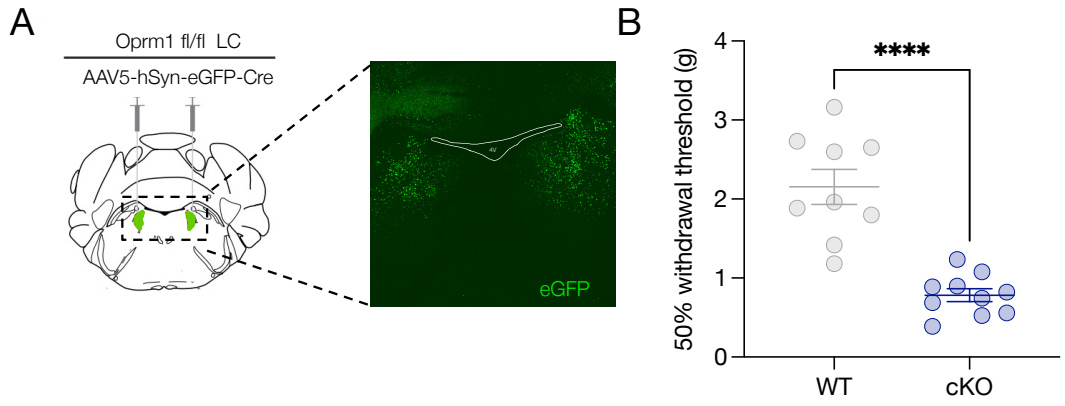

Supplementary Figure 6. Local LC site-selective Cre delivery in adult *oprm1*$^{fl/fl}$ mice maintains the same basal hypersensitivity as *Oprm1*$^{fl/fl}$x*Dbh*$^{Cre+/-}$ mice. (**A**) Viral strategy for *oprm1* deletion in the adult LC. eGFP=Cre. (**B**) *oprm1* deletion in the LC decreases baseline 50% mechanical withdrawal threshold. Data expressed as mean +/- SEM, n=9-10/group, unpaired t-test, ****p<0.0001.

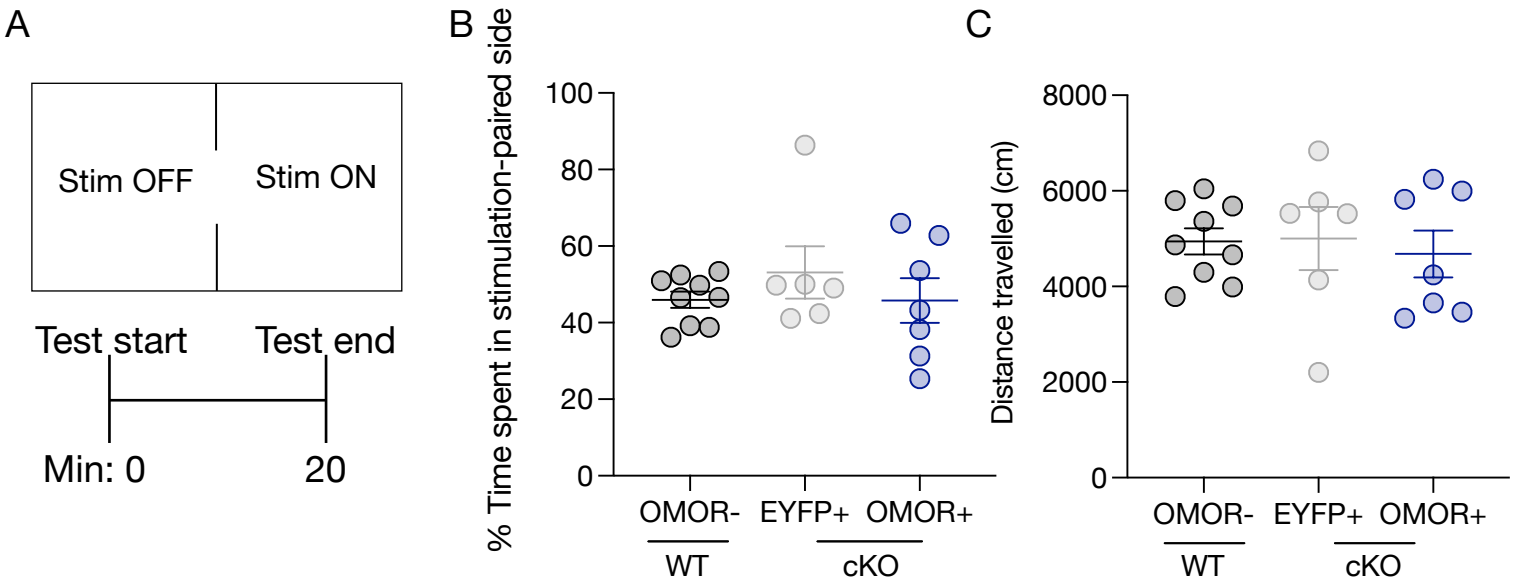

Supplementary Figure 7, Activation of Opto-MOR signaling in the LC of *Oprm1*$^{fl/fl}$x*Dbh*$^{Cre+/-}$ mice does drive a real-time place preference or alter locomotor behavior. (**A**) Real-time place testing schematic and experimental timeline. (**B**) % time spent in stimulation-paired side of real-time place testing apparatus shows no significant difference between groups. Data expressed as mean +/- SEM, n=7-10/group, one-way ANOVA. (**C**) Distance travelled during real-time place test shows no significant effect of opto-MOR stimulation. Data expressed as mean +/- SEM, n=7-10/group, one-way ANOVA.

Supplementary Figure 7